DØ Note 4759
4th July 2005

Search for the Higgs boson in $H \rightarrow WW^{(*)} \rightarrow \ell^+\nu\ell'^-\bar{\nu}$ $(\ell, \ell' = e, \mu, \tau_{lep})$ decays at DØ in Run II

Johannes Elmsheuser
Ludwig-Maximilians-Universität München, Germany
elmsheus@fnal.gov

Marc Hohlfeld
Johannes Gutenberg-Universität Mainz, Germany
hohlfeld@fnal.gov

Draft 2.2

Abstract

We present a search for the Higgs boson in $H \rightarrow WW^{(*)} \rightarrow \ell^+\nu\ell'^-\bar{\nu}$ $(\ell, \ell' = e, \mu, \tau_{lep})$ decays in $p\bar{p}$ collisions at a center-of-mass energy of $\sqrt{s} = 1.96$ TeV. The data, collected from April 2002 to June 2004 with the Run II DØ detector, correspond to an integrated luminosity of 325 pb^{-1} in the e^+e^-, 318 pb^{-1} in the $e^\pm\mu^\mp$ and 299 pb^{-1} in the $\mu^+\mu^-$ final state. The number of events observed is consistent with expectations from standard model backgrounds. Limits from the combination of all three channels on the production cross section times branching ratio $\sigma \times BR(H \rightarrow WW^{(*)})$ are presented.

1 Introduction

The present note describes the search for the Higgs boson in $H \to WW^{(*)} \to \ell^+\nu\ell'^-\bar{\nu}$ ($\ell, \ell' = e, \mu, \tau_{lep}$) decays in data collected by the DØ experiment at the Fermilab Tevatron collider at a center of mass energy of $\sqrt{s} = 1.96$ TeV. The final states of these processes are characterized by two isolated leptons (e or μ) with high transverse momentum p_T and a significant missing transverse energy originating from the undetected neutrinos. For further phenomenological discussions the reader is referred to [1]. It is assumed that the reader is familiar with the DØ detector [2].

Not all aspects of the analysis are discussed in detail. The reader is referred to the analysis note [3] and publication [4] describing the measurement of the WW production cross section using the same three final states. The same techniques and methods have been used for the following search for the Higgs boson.

The following sections describe the data and Monte Carlo (MC) samples and various efficiency determinations. Furthermore a detailed description of a Higgs boson mass dependent event selection is given. Various systematic errors have been studied. The final section provides a presentation of the limits on the cross section times branching ratio $\sigma \times BR(H \to WW^{(*)})$ for the combination of all three channels.

1.1 Higgs production and decay

For standard model Higgs boson decays in the $H \to WW^{(*)}$ channel, the cross section multiplied by the branching ratio is largest for masses near $m_H = 160$ GeV. Figure 1 shows the production cross section (top left) and the branching ratio (top right) as a function of the Higgs boson mass. However, since it is only of the order of a few fb, the present data, corresponding to an integrated luminosity of 300–325 pb^{-1}, have no sensitivity to a standard model Higgs boson. The present lower limit on the mass of a standard model Higgs bosons from searches at the electron–positron collider LEP is $m_H > 114.4$ GeV [5].

Event rates are expected to be larger in alternative models, where either the production cross section or the branching fraction into W pairs is enhanced. Such scenarios are realized, for example, in a fourth–generation model, where the Higgs production cross section is about a factor of 8.5 larger in the mass range 100 GeV $< m_H <$ 200 GeV [6]. In Fig. 1 (bottom), the enhancement factor for a fourth–generation model is shown as a function of the mass of the Higgs boson. The enhancement factor depends on the Higgs mass and on the masses of the quarks of the hypothetical fourth generation.

The cross sections multiplied by the branching ratio $\sigma\times$ BR($H \to WW^{(*)} \to \ell^+\nu\ell'^-\bar{\nu}$) for the standard model Higgs boson are given in Table 1, assuming the usual three generations, as well as an additional fourth generation of particles. The QCD–corrected results are taken into account at NLO for the gluon fusion process [7]. The enhancement

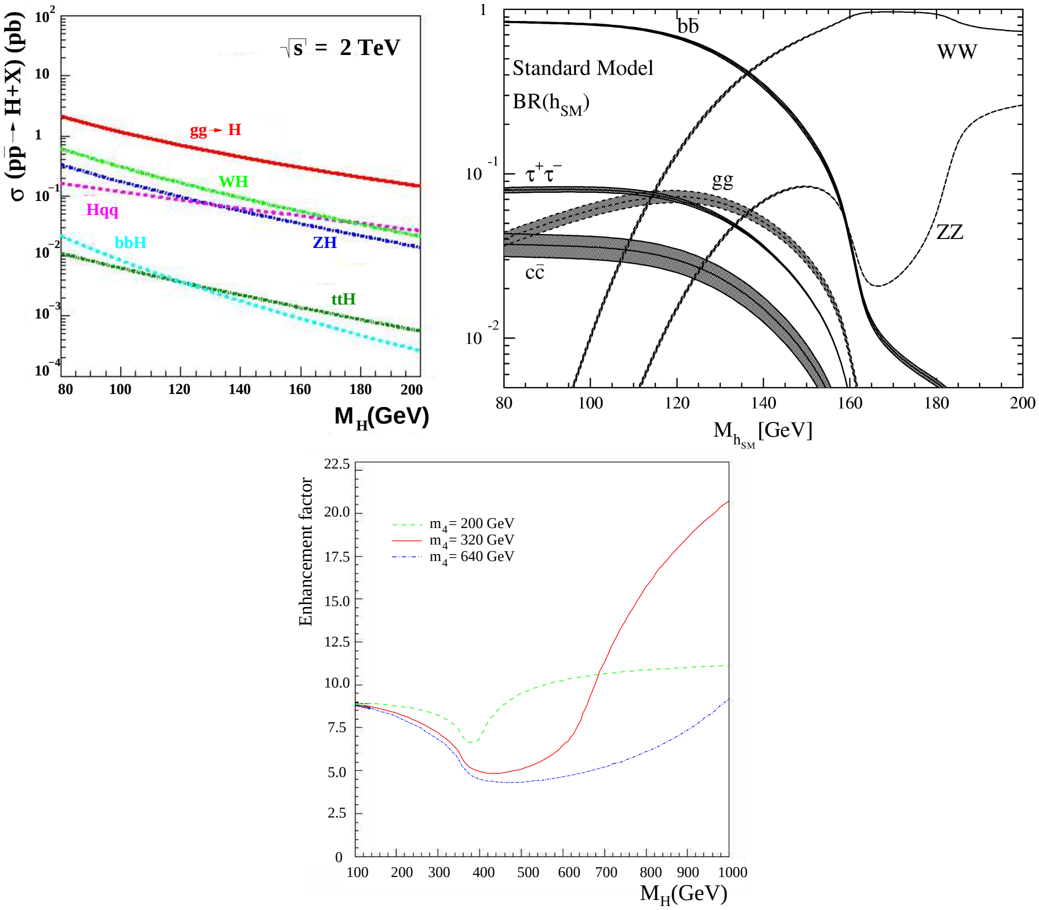

Figure 1: Standard model Higgs boson production cross section (top left) and the branching ratio (top right). The enhancement factor for the Higgs boson production from gluon fusion via loops due to a fourth family of quarks [6] (bottom).

factor from the fourth generation changes slightly for $m_H < 300$ GeV, but is assumed to be ≈ 8.5 for the mass range under consideration. This enhancement factor corresponds to a Higgs boson of $m_H = 160$ GeV, and a mass of $m_4 = 320$ GeV for the fourth generation quarks. The current mass limit for a fourth generation is $m_4 = m_{b'} > 199$ GeV [8]. This limit is model dependent and assumes a 100% branching ratio $b' \to bZ$.

2 Data sample and efficiencies

This analysis uses data collected at a center of mass energy of $\sqrt{s} = 1.96$ TeV by the DØ experiment between April 2002 and June 2004. The total integrated luminosity analyzed is in the range of $\mathcal{L} \approx 299 - 325\ pb^{-1}$ depending on the final state. For the e^+e^- final state the 2EM [9] skim is used whereas for the $e^\pm\mu^\mp$ channel the EMMU [9]

m_H(GeV)		100	120	140	160	180	200
$\sigma\times$BR (pb)	SM	0.011	0.089	0.207	0.256	0.181	0.101
	4^{th} Gen	0.066	0.471	1.217	2.017	1.471	0.804

Table 1: $\sigma\times$ BR for the Higgs boson in the channel $H \to WW^{(*)}$ in the mass range 100 GeV $< m_H <$ 200 GeV. The calculations are given for the standard model Higgs and for the model with a fourth generation.

skim is used. The analysis in the $\mu^+\mu^-$ channel is based on the 2MU [9] skim. The events are reconstructed with different versions of p14 of dØreco. Approximately 22% of the data are reconstructed with version p14.03 of dØreco, 27% with p14.05 and 50% with p14.06. All events have been fixed for different reconstruction deficits (pass 1 of the TMB fixing) [9] and have been processed with `dØcorrect` v6 [9].

A detailed discussion of the data samples, comparison between data and Monte Carlo efficiencies, different efficiencies of electron and muon reconstruction, trigger studies, track match and likelihood are described in [10, 11]. In these references a discussion of luminosity determination as well as corrections applied to the Monte Carlo to match the data can also be found. In addition a study of trigger efficiencies for the e^+e^- final state can be found in [12]. Further studies of the trigger and object ID performances for electrons and muons are describes in [13, 14].

3 Object identification

3.1 Electron identification

Two electromagnetic objects with $p_T > 7$ GeV and $|\mathrm{ID}| = 10$, 11 are required in the 2EM skim. The offline selection in the EMMU skim requires one reconstructed EM object with $p_T > 5$ GeV.

The transverse momentum measurement of the electrons is based on calorimeter cell energy information. The corrections for calorimeter non–linearity and energy corrections depending on the geometry are applied to the EM clusters [15]. All data are fixed for energy sharing, cable swaps and tower 2 problems [9].

Electrons are selected following the standard electron identification criteria [15]:

- $|\mathrm{ID}| = 10$, 11
- Isolation: ISO < 0.15
- Electromagnetic fraction: EMF > 0.90

- Shower shape χ^2 (HMatrix): HMx8 < 50.0

To further reduce contamination from jets in the electron sample and to distinguish between electrons and photons a likelihood estimator is used. This likelihood combines information from the calorimeter and track information [16]. The electromagnetic fraction and HMatrix enter the likelihood as well as E/p, spatial χ^2, track isolation and DCA. To select good electrons a value of 0.3 is used for the likelihood criterion. All electrons are restricted to $\mid \eta_{det} \mid < 3.0$.

Since the efficiencies in the Monte Carlo overestimate the efficiencies in the data, the Monte Carlo is corrected for this effect. The correction factor for electrons for the likelihood criterion in the CC is found to be 0.933 ± 0.010 while it is 0.785 ± 0.014 in the EC. A more detailed discussion on electron efficiencies can be found in [12]. Within the errors this numbers are compatible with the numbers from [10].

3.2 Muon identification

For the EMMU skim one loose muon with $p_T > 5$ GeV is required whereas for the 2MU skim two loose muons without p_T requirement must be found in the event.

For this analysis the following selection criteria are applied:

- Loose muon criteria
- Match to a central track
- The transverse momentum measurement is based on the track measurement provided by the central tracking system (CFT+SMT)
- Track isolation $\sum_{\text{tracks}}^{\mathcal{R}<0.5} p_T < 4.0$ GeV
- Timing cut in A and BC layers to reject cosmics
- Constraint to primary vertex

$$(d0^{\mu}_{\text{Vtx}}/0.16\,\text{cm})^2 + (z0^{\mu}_{\text{Vtx}}/0.5\,\text{cm})^2 < 1. \tag{1}$$

All muons are restricted to the coverage of the muon system, namely $|\eta| < 2$. To get better resolution for "CFT-only" tracks the p_T for the muon is recalculated using the primary vertex as a constrained if no hits are found in the SMT.

Since the efficiencies in the Monte Carlo overestimate the efficiencies in the data, the Monte Carlo is corrected for this effect. The combined correction factor for muon identification, tracking and isolation is found to be 0.945 ± 0.017. A more detailed discussion and comparison between muon identification in data and Monte Carlo is presented in [11].

3.3 Jet identification

Jets are selected following the recommendations of the Jet algorithm group [17]. They are reconstructed using the Run II cone jet algorithm with a cone radius $R = 0.5$ and corrected with the jet energy scale correction `jetcorr` v5.3 [18]. The jet identification criteria are

- Electromagnetic fraction: 0.05 < EMFraction < 0.95
- Coarse hadronic fraction: CHF < 0.4
- Ratio of energies of hottest and next–to–hottest cell: Hot fraction < 10
- Number of towers containing more than 90% of the energy: n90 > 1
- Level 1 confirmation: l1set / (p_T^{jet} · (1 - CHF)) > 0.4 (in CC, EC) or > 0.2 (ICD)

l1set is the sum of the Level 1 calorimeter tower energies in a cone of $\Delta\mathcal{R} < 0.5$ around the jet axis. The jets have to be in the pseudo-rapidity range of -2.5 to $+2.5$.

3.4 Missing transverse energy $\not{E}_T$

Following the recommendations of the Jet/Missing Energy algorithm group the missing energy is recalculated using all calorimeter cells with an energy above 0 MeV where the unclustered energy in the coarse hadronic layers is excluded except for coarse hadronic cells which belong to a jet [17]. After that a jet energy scale correction is applied [18] and post processed by `dØcorrect`. The variable `MetbCorrCaloMu` includes all corrections for the coarse hadronic layer, electrons from jet removal, jet energy scale correction, electron, and muon corrections. This variable is recalculated applying the muon quality criteria described in section 3.2.

4 Trigger

4.1 The e^+e^- final state

For the di–electron final state, a combination of single– and di–electron triggers is used. A detailed study of the trigger efficiency can be found in [12]. For the parameterization of the turn-ons, the following function is used:

$$\epsilon_{tr}(p_T) = O + 0.5 \cdot P_2 \cdot \left(1 + Erf\left(\frac{p_T - H_2}{\sqrt{p_T} \cdot S_2}\right)\right) + 0.5 \cdot P_1 \cdot \left(1 + Erf\left(\frac{p_T - H_1}{\sqrt{p_T} \cdot S_1}\right)\right) \quad (2)$$

Trigger version		O	P_2	H_1	H_2	S_1	S_2
v5–v11	e_1	0.0	0.490	14.13	8.84	0.49	0.26
v5–v11	e_2	0.279	—	9.11	—	0.36	—
v12	e_1	0.0	0.78	11.67	7.73	0.0001	0.12
v12	e_2	0.592	—	9.04	—	0.25	—

Table 2: Parameters for the trigger turn-ons of the e^+e^- final state. All values are taken from Ref. [12].

The parameters H_1 and H_2 are the half points, S_1 and S_2 the slopes, P_2 and $P_1 = 1 - P_2 - O$ the plateaus, and O is the offset. All values are fitted separately for leading and next-to-leading electron as well as for the trigger version v5–v11 and v12. The parameters are listed in Table 2.

4.2 The $e^{\pm}\mu^{\mp}$ final state

Separate studies for electron and muon part of the electron–muon trigger have been performed. The studies for the electron part can be found in [10]. The trigger is nearly fully efficient for electrons with $p_T > 15$ GeV. To take into account small inefficiencies, events with electrons with $p_T < 17$ GeV (16 GeV) are down-scaled by a factor of 0.91 (0.98) for trigger versions v5–v11 (v12).

For the muon part, the studies of [19] are used. The η distribution of the muons is parameterized with the following function:

$$\epsilon_{tr}(\eta) = A_3 + A_0 \cdot exp\left(-A_1 \cdot \left(\eta^2 - A_2^2\right)\right) \cdot \sin\left(\eta^2 - A_2^2\right) \tag{3}$$

with $A_0 = -0.8$, $A_1 = 2.8$, $A_2 = 0.1$, and $A_3 = 0.99$.

4.3 The $\mu^+\mu^-$ final state

In the di–muon selection events have been triggered by one of the five triggers: 2MU_A_L2M0, 2MU_A_L2ETAPHI, 2MU_A_L2M0_TRK10, 2MU_A_L2M0_TRK5 or MUW_W_L2M3_TRK10. These triggers are required to be not prescaled and to have a good luminosity block number. The trigger efficiency for the first triggers has been determined in Reference [11]. The L3 efficiency for the trigger 2MU_A_L2M0_TRK5 has been calculated to be 79% (assuming 2MU_A_L2M0 is 100%). To determine the latter efficiency events have been selected that fulfill the trigger criteria on Level 1 and 2 and subsequently have been tested whether they meet the Level 3 conditions. The corresponding dataset for the trigger 2MU_A_L2M0_TRK5 is 31% for the whole dataset. Therefore the overall trigger efficiency has to be corrected with $\epsilon = 0.94$.

With the addition of the single muon trigger MUW_W_L2M3_TRK10 the efficiency loss ϵ due to the 2MU_A_L2M0_TRK5 trigger is compensated.

5 Monte Carlo signal and background

MC samples

All simulated events are generated using PYTHIA 6.202 [20] and ALPGEN [21] using the CTEQ5L parton distribution functions [22]. They are processed through a full detector simulation with an overlaid Poisson–distributed average of 0.8 minimum bias events. A top quark mass of $m_t = 175$ GeV is used. Table 3 gives an overview of all Monte Carlo samples with their cross sections and references used in comparisons with data. The contribution from QCD events was estimated from data (see Section 6). The background processes listed in Table 3 together with the multi–jet background are referred to as standard model backgrounds later on. A more detailed description of the Monte Carlo samples used in the e^+e^- and $e^\pm\mu^\mp$ analysis is presented in [10]. The Monte Carlo samples used in the $\mu^+\mu^-$ channel and a description of background determination from data can be found in [11].

Process		$\sigma \times BR$ [pb]	Ref.
$Z/\gamma^* \rightarrow ll \quad (\ell = e, \mu, \tau)$	$15\,\text{GeV} < m_{\ell\ell} < 60\,\text{GeV}$	465	[23]
	$60\,\text{GeV} < m_{\ell\ell} < 130\,\text{GeV}$	254	[23]
	$130\,\text{GeV} < m_{\ell\ell} < 250\,\text{GeV}$	2	[23]
$W \rightarrow \ell\nu$ inclusive $(\ell = e, \mu)$		2717	[23]
$WW \rightarrow \ell\nu\ell\nu$ $(\ell = e, \mu)$		0.147	[24]
$WZ \rightarrow \ell\nu\ell\ell$ $(\ell = e, \mu)$		0.014	[24]
$ZZ \rightarrow \ell\ell\ell\ell$ $(\ell = e, \mu)$		0.002	[24]
$t\bar{t} \rightarrow b\ell\nu b\ell\nu$ $(\ell = e, \mu)$		0.076	[26]
Υ(1s)$\rightarrow \ell\ell$		27	[20]
Υ(2s)$\rightarrow \ell\ell$		20	[20]
$H \rightarrow WW^{(*)} \rightarrow \ell^+\nu\ell'^-\bar{\nu}$	$(m_H = 100\,\text{GeV})$	0.00108	[27, 28]
$H \rightarrow WW^{(*)} \rightarrow \ell^+\nu\ell'^-\bar{\nu}$	$(m_H = 120\,\text{GeV})$	0.00855	[27, 28]
$H \rightarrow WW^{(*)} \rightarrow \ell^+\nu\ell'^-\bar{\nu}$	$(m_H = 140\,\text{GeV})$	0.01971	[27, 28]
$H \rightarrow WW^{(*)} \rightarrow \ell^+\nu\ell'^-\bar{\nu}$	$(m_H = 160\,\text{GeV})$	0.02421	[27, 28]
$H \rightarrow WW^{(*)} \rightarrow \ell^+\nu\ell'^-\bar{\nu}$	$(m_H = 180\,\text{GeV})$	0.01701	[27, 28]
$H \rightarrow WW^{(*)} \rightarrow \ell^+\nu\ell'^-\bar{\nu}$	$(m_H = 200\,\text{GeV})$	0.00936	[27, 28]

Table 3: Cross section times branching ratio for the various Monte Carlo samples and their references, used in comparisons with data.

Jet re-weighting

The jet multiplicities for Z/γ^* production are underestimated in the Monte Carlo. Thus re-weighting factors are obtained by a comparison of the jet multiplicities in data and Monte Carlo. To account for the underestimation in the Monte Carlo in the e^+e^-, $e^\pm\mu^\mp$, and $\mu^+\mu^-$ channel, the $Z/\gamma^* \to ee$, $Z/\gamma^* \to \mu\mu$, and $Z/\gamma^* \to \tau\tau$ events are re-weighted as a function of Z/γ transverse momentum using the formula [29]

$$reweightfactor = 1.302/(1. + exp(-(2.053 - p_T^{Z/\gamma}) \cdot 0.4115)) \ . \tag{4}$$

For the $e^\pm\mu^\mp$ final state the re-weighting does not have a significant influence since no large backgrounds from $Z/\gamma^* \to ee$ and $Z/\gamma^* \to \mu\mu$ events are present.

Electron and muon momentum resolution

The momentum resolution for electrons and muons in the data is not correctly described by the Monte Carlo simulation. Thus an additional smearing has to be applied in the Monte Carlo.

The p_T of the electrons is replaced by $p_T \to p_T{\cdot}c \cdot (1 + Gauss(0, f))$ where $Gauss(0, f)$ is the smearing parameter, which is randomly chosen from a Gaussian distribution with mean 0 and width f and c is an overall calibration factor. The values for f and c depend on the region of the detector. The following values are used in the analysis [30]:

- central calorimeter: $f = 0.045$, $c = 1.003$ ($\mid \eta_{det} \mid < 1.1$)
- endcaps: $f = 0.034$, $c = 0.996$ ($1.5 < \mid \eta_{det} \mid < 2.5$)
- non fiducial regions: $f = 0.115$, $c = 0.950$

Also for muons the Monte Carlo does not describe the muon resolution in the data. Thus again the p_T of the muons is smeared in the Monte Carlo. Unlike the electrons the smearing is applied to $1/p_T$. In the $e^\pm\mu^\mp$ and $\mu^+\mu^-$ channel, the muons are smeared using $1/p_T \to 1/p_T+$ (A+B/p_T)$\cdot$ Gauss(0,1) with A = 0.0013(0.0023) and B = 0.017(0.028) for tracks with (without) SMT hits [31].

γ conversions

The γ conversion probability in the Monte Carlo is not properly modeled. This may lead to an underestimation of the $W(\to e, \mu) + \gamma$ contribution to the background. To compensate this underestimation, $W + \gamma$ events with less than 5 hits for the electron track are re-weighted with a factor of 2.5, if any of the electrons in the e^+e^- or $e^\pm\mu^\mp$ channel are matched with a photon in the MCKineChunk and the number of SMT hits for the track is less than 5. A more detailed study of this issue is presented in [12].

6 QCD and $W + jets$ Background determination

The following section describes determination of the QCD background from data for the e^+e^- and $e^\pm\mu^\mp$ final states. The subsequent section describes the determination of the QCD and $W + jets$ background from data and MC for the $\mu^+\mu^-$ final state.

6.1 QCD background in the e^+e^- and $e^\pm\mu^\mp$ final states

The background contribution from multi–jet production was determined directly from DØ data. The same 2EM and EMMU skim are used again to obtain a sample of EM–like jets. All electron identification and p_T selections are applied, as indicated before, but with the HMatrix and Likelihood criteria inverted for the EM candidates. That is, requiring poor electrons, or

$$\text{HMx8} \ > \ 50 \qquad \text{or}(ee)/\text{and}(e\mu) \qquad \text{Likelihood} < 0.3 \tag{5}$$

for the EM cluster. This reduces greatly true electrons in the sample. Because of the small fake probability, each of the poor electrons has to pass only one of the inverted electron quality cuts for the di–electron QCD sample. For the $e^\pm\mu^\mp$ final state, the muon has to fail a calorimeter isolation criterion of

$$E(\Delta\mathcal{R} < 0.4) - E(\Delta\mathcal{R} < 0.1) \ < \ 2.5\text{GeV} \tag{6}$$

to reject contributions from $W(\to \mu)+jets/\gamma$ events in the QCD sample. This selection is referred as the fake sample later on. To use the method described in the following it is assumed that the ratio of like–sign to unlike–sign events in the fake sample and in the QCD contribution to the search sample is equal.

To get an estimate for the QCD contribution in the search sample (with HMx8 < 50 and Likelihood > 0.3), a region in phase space is used where this background is expected to be dominant. This has to be done because otherwise an over– or underestimation of efficiencies could be absorbed in the normalization of the multi–jet background.

A sample of like-sign leptons offers a good possibility for the normalization because most of the standard model backgrounds as well as the signal have leptons of opposite charge in the final state. Thus they only contribute to the like-sign sample if one of the lepton charges is mis-measured. Other contributions are expected from $W + jet/\gamma$ events, because the charge of the mis-measured jet or converted electron is arbitrary. This is also the case for the multi–jet background. Hence approx. 50% of this background are expected in the like–sign sample.

Since no cut on the missing transverse energy is applied, the fake sample is dominated by multi–jet events. The contribution from $W + jet$ events is negligible.

The absolute normalization of the multi–jet background is done as follows. The number $N^{\pm\pm}_{search}$ of like-sign events in the search sample is determined from which the expected contribution $N_{MC}^{\pm\pm}$ from all standard model backgrounds (see Table 3) except the multi–jet background is subtracted. The excess

$$N_{QCD}^{\pm\pm} = N_{search}^{\pm\pm} - N_{MC}^{\pm\pm} \tag{7}$$

of events corresponds to the multi–jet contribution in like-sign events in the search sample.

For the e^+e^- channel the number of like–sign events in the search sample is found to be $N_{search}^{\pm\pm} = 1519$ events. The prediction from standard model backgrounds (without multi–jet events) is $N_{MC}^{\pm\pm} = 1210$ events which is dominated from $Z/\gamma^* \to ee$ contributions where one of the electron charges is mis-measured. In the $e^\pm\mu^\mp$ channel the number of like-sign events in the search sample is $N_{search}^{\pm\pm} = 210$, while non QCD contributions from the Monte Carlo are expected to be $N_{MC}^{\pm\pm} = 55$ events. Most of these events are from $W + jet/\gamma$ contribution.

A normalization factor for the QCD sample

$$f_{Norm}^{QCD} = \frac{N_{search}^{\pm\pm} - N_{MC}^{\pm\pm}}{N_{fake}^{\pm\pm}} = \frac{N_{QCD}^{\pm\pm}}{N_{fake}^{\pm\pm}} \tag{8}$$

is obtained, where $N_{fake}^{\pm\pm}$ is the number of like-sign events in the fake sample.

The number of multi–jet events $N_{QCD}^{\pm\mp}$ in the unlike-sign search sample can be computed from the number $N_{fake}^{\pm\mp}$ of events in the unlike-sign fake sample using the equation

$$N_{QCD}^{\pm\mp} = f_{Norm}^{QCD} \cdot N_{fake}^{\pm\mp} \ . \tag{9}$$

To get an estimate for the multi–jet background after each selection criterion the normalization factor f_{Norm}^{QCD} is determined once after the preselection and is then kept constant. The rejection factors η_{QCD}^i of the selection criteria, where i corresponds to the i^{th} selection criterion, are determined using the fake sample. The rejection factors η_{QCD}^i can be obtained via the expression

$$\eta_{QCD}^i = \frac{\text{Number of multi}-\text{jet events after selection criterion } i}{\text{Number of multi}-\text{jet events after preselection}} = \frac{N_{fake}^{i\pm\mp}}{N_{fake}^{\pm\mp}} \ . \tag{10}$$

Accordingly, the number of multi–jet events $N_{QCD}^{i\pm\mp}$ in the search sample after the selection criterion i is applied is given by

$$N_{QCD}^{i\pm\mp} = f_{Norm}^{QCD} \cdot \eta_{QCD}^i \cdot N_{fake}^{\pm\mp} \ . \tag{11}$$

Figure 2 shows the invariant mass m_{ee} (left) and transverse opening angle $\Delta\phi_{ee}$ distribution (right) of like-sign events in the e^+e^- search sample and the expected background contributions after the electron identification criteria and p_T cuts of 15 GeV and 10 GeV are applied. Also, the multi–jet contribution is shown in these plots using the method described above. In Fig. 3 the $\Delta\phi_{e\mu}$ distribution for like-sign leptons for the $e^\pm\mu^\pm$ final state is shown.

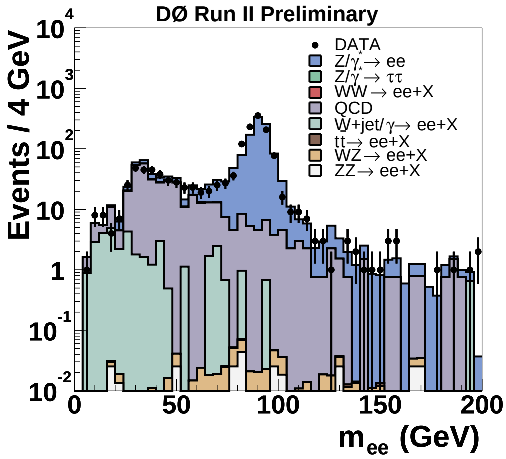

Figure 2: Distribution of the invariant mass m_{ee} (left) and the transverse opening angle $\Delta\phi_{ee}$ (right) after electron ID and p_T cuts for like-sign events for the ee final state.

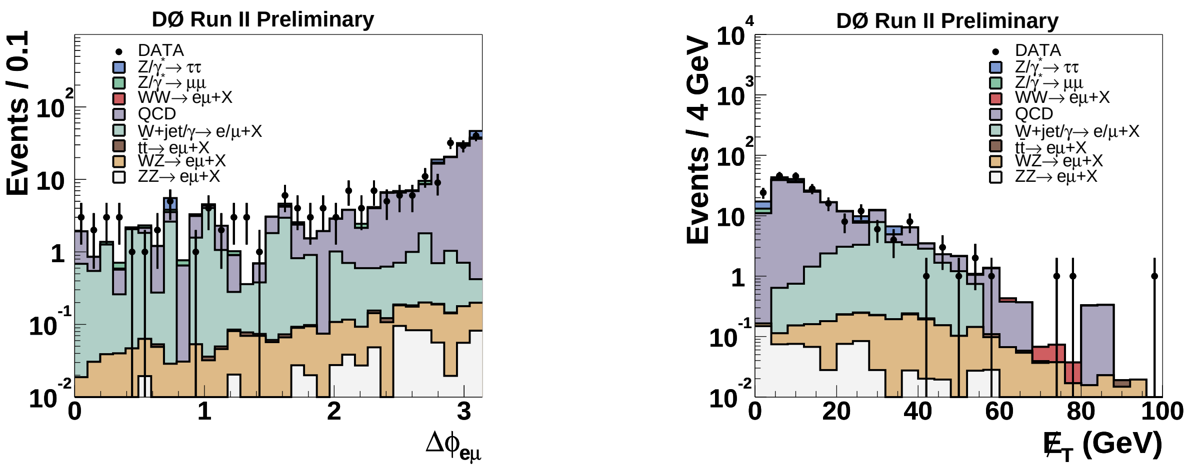

Figure 3: Distribution of the transverse opening angle $\Delta\phi_{e\mu}$ (left) and the missing transverse energy $\not{E}_T$ (right) after lepton ID and p_T cuts for like-sign events for the $e\mu$ final state.

6.2 QCD and W+jets background in the $\mu^+\mu^-$ final state

The contribution from $b\bar{b}$ and $W + jets$ background is determined from data and MC. A sample of $b\bar{b}$ events was generated using PYTHIA. EvtGen [32] and `d0_mess` [33] were used for proper decay description and statistical enhancement.

The contribution from $b\bar{b}$ events is estimated in data from like-sign di–muon events with an inverted isolation criterion. One muon has to fail the isolation cuts, i.e. track isolation: $\sum_{tracks}^{R<0.5} p_{\mathrm{T}} > 4.0\,\mathrm{GeV}$. By inverting the muon isolation criterion in the like-sign case an enriched sample of QCD and $W + jets$ events with almost no $Z/\gamma^* \to \mu\mu$ contribution is selected. Figure 4 shows the distributions of the di–muon invariant mass, the muon transverse momentum p_T, the di–muon opening angle $\Delta\phi$ and the missing transverse energy in the like-sign di–muon sample. This background is characterized by low muon p_T, large opening angle and a modest missing transverse energy. The ratio

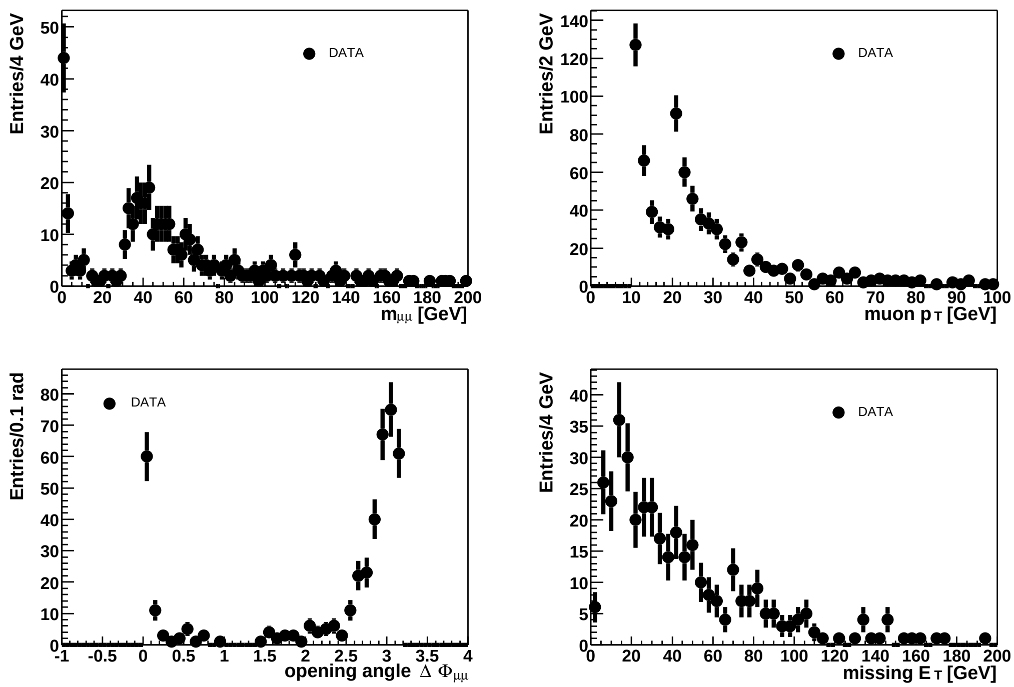

Figure 4: Distributions of the di–muon invariant mass, the muon transverse momentum, di–muon opening angle $\Delta\phi$ and the missing transverse energy from QCD and $W + jets$ background enriched sample.

between like-sign and non like-sign $b\bar{b}$ events is obtained from MC to be ≈ 0.344. The number of $b\bar{b}$ events is given by the number of non like-sign events in MC ($N_{\rm all}^{\rm MC,ULS}$) times the isolation efficiency $\varepsilon_{\rm iso,b\bar{b}}$ and normalized to the data by the ratio of inverted isolated like-sign events in data and MC:

$$N_{\rm b\bar{b}} = \varepsilon^2_{\rm iso,b\bar{b}} \cdot \frac{N_{\rm inviso}^{\rm DATA,LS}}{N_{\rm inviso}^{\rm MC,LS}} \cdot N_{\rm all}^{\rm MC,ULS}. \tag{12}$$

The isolation efficiency is determined by the number of isolated muons divided by the number of all muons in the MC sample: $\varepsilon_{\rm iso,b\bar{b}} = \frac{N^{\mu}_{\rm iso,b\bar{b}}}{N^{\mu}_{\rm all}} = 0.068 \pm 0.001(stat.) \pm 0.006(sys.)$. The cut on the muon transverse momentum was varied in a range of $\Delta p_{\rm T} = 3\,{\rm GeV}$ since muons with smaller $p_{\rm T}$ tend to be less isolated. Table 4 shows the contribution of $b\bar{b}$ events after different successive cuts described in section 7. Since the numbers are very similar within the errors for all Higgs mass m_H dependent selections, Table 4 shows only the numbers of the m_H= 160 GeV selection. Already after the preselection the number of $b\bar{b}$ events is very small.

	$N_{\rm inviso}^{\rm DATA,LS}$	$N_{\rm inviso}^{\rm MC,LS}$	$N_{\rm all}^{\rm MC,ULS}$	$N_{\rm b\bar{b}}$
Cut 1	2839	6285	19372	40.3 ± 4.1
Cut 2	1138	728	2153	15.5 ± 1.7
Cut 3	88	60	110	0.7 ± 0.3
Cut 4	48	27	25	0.2 ± 0.1
Cut 5	28	10	11	0.1 ± 0.1
Cut 6	16	9	8	0.1 ± 0.1
Cut 7	10	9	8	0.1 ± 0.1
Cut 8	6	8	8	0.1 ± 0.1

Table 4: $b\bar{b}$ contribution estimated from like-sign di–muon events in data for a Higgs boson mass m_H= 160 GeV selection.

The number events from W+$b\bar{b}$ production is obtained directly from MC using Pythia. The normalization of the sample is done with a cross-section $\sigma \approx 4.55$ pb calculated with COMPHEP [34]. This cross-section predicted by Pythia is $\sigma \approx 4.6$ pb. Due to the large theoretical uncertainties a systematic error of 100% is assigned to this cross-section. After all cuts the contribution from W+$b\bar{b}$ production is approximately the same as from $b\bar{b}$ production.

A systematic check of the W+jet production is performed using Alpgen [21] instead of the Pythia Monte Carlo generator. Different processes for one- and two-jet production with charm and bottom quarks and inclusive jet production have been simulated: W+ 1 jet, W+2 jets, W+ 1 charm jet, W+ 1 jet+ 1 charm jet, W+ 2 charm jets, W+ 2 bottom jets. After all cuts only W+2 charm jets and W+ 2 bottom jets production show measurable contribution of 0.1 ± 0.1 events and are in good agreement with the numbers obtained using Pythia.

7 Selection of the signal

Among the three different final states a common Higgs mass m_H dependent selection has been developed. This selection will be explained in the next section, whereas the specific details of the three individual channels and the cut flows are discussed in the subsequent sections.

To get the best expected limit, a five-dimensional scan in the plan $\not\!\!E_T$, $\not\!\!E_T^{\rm Sc}$, $m_{e\mu}$, $m_T^{e\mu}$, and $p_T^e + p_T^\mu + \not\!\!E_T$ is performed. As signal, a mass of $m_H = 160$ GeV is chosen, because the best limits are expected in this mass region. For the same reason, the $e^\pm\mu^\mp$ final state is used, since it has the best sensitivity. The optimal selection is then copied for the other Higgs masses and final states. As an example, the result of the scan in the two-dimensional plane lower cut($p_T^e + p_T^\mu + \not\!\!E_T$)–upper cut($p_T^e + p_T^\mu + \not\!\!E_T$) is shown in Fig. 5. It can be seen, that the best expected limit is achieved for a cut of 100 GeV $<$ $p_T^e + p_T^\mu + \not\!\!E_T < 160$ GeV.

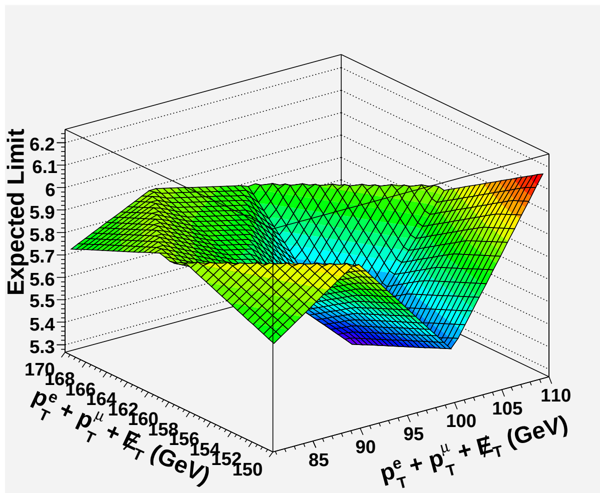

Figure 5: Expected limit as function of the variation of the lower and upper cut value of the variable $p_T^e + p_T^\mu + \not\!\!E_T$.

7.1 A common selection

To exploit the full kinematic range that changes with increasing Higgs mass various cuts are used dependent on the Higgs mass m_H. Events must fulfill specific trigger and object ID criteria described in the following sections.

- In all three channels, two leptons originating from the same vertex are required to be of opposite charge, and must have $p_T > 15$ GeV for the leading lepton and $p_T > 10$ GeV for the trailing one (Cut 1).

- To suppress backgrounds with similar event topologies as $H \to WW^{(*)}$ production a set of cuts is applied as follows: In all cases, the background is largely dominated by Z/γ^* production which is suppressed by requiring the $\not\!\!E_T$ to be greater than 20 GeV (Cut 2).

- Events are also removed if the $\not\!\!E_T$ has a large contribution from the mis-measurement of jet energy, using the following procedure. The fluctuation in the measurement of jet energy in the transverse plane can be approximated by $\Delta E^{\mathrm{jet}} \cdot \sin\theta^{\mathrm{jet}}$ where ΔE^{jet} is proportional to $\sqrt{E^{\mathrm{jet}}}$. The opening angle $\Delta\phi\,(\mathrm{jet}, \not{E}_T)$ between this projected energy fluctuation and the missing transverse energy provides a measure of the contribution of the jet to the missing transverse energy. The scaled missing transverse energy defined as

$$\not{E}_T^{\mathrm{Sc}} = \frac{\not{E}_T}{\sqrt{\sum_{\mathrm{jets}} \left(\Delta E^{\mathrm{jet}} \cdot \sin\theta^{\mathrm{jet}} \cdot \cos\Delta\phi\,(\mathrm{jet}, \not{E}_T)\right)^2}} \tag{13}$$

is required to be greater than 15 (Cut 3).

- Additional cuts are applied to further reduce the Z/γ^* background and other backgrounds. Since the charged lepton system and the two neutrinos are emitted back–to–back, the invariant mass for the Higgs decays is restricted to $m_H/2$. Thus, depending on the Higgs mass m_H the invariant mass $m_{\ell\ell}$ is required to be $m_{\ell\ell} < m_H/2\,\mathrm{GeV}$ (Cut 4). In the $\mu^+\mu^-$ channel a lower cut boundary with $m_{\ell\ell} > 20\,\mathrm{GeV}$ is required to remove events from J/ψ and Υ production. Figure 6 shows the invariant mass distribution for the six different Higgs masses in the $e^\pm\mu^\mp$ channel.

- The sum of the lepton transverse momentum p_T and the missing transverse momentum $\not{E}_T$ is required to be in the range $m_H/2 + 20(10)\,\mathrm{GeV} < p_T^{\ell_1} + p_T^{\ell_2} + \not{E}_T < m_H$ for the e^+e^- and $e^\pm\mu^\mp$ channel ($\mu^+\mu^-$ channel) (Cut 5). The distribution of this variable for the different Higgs masses is presented in Fig. 7 for the signal after application of the invariant mass cut.

- Because of the neutrinos in the final state, the Higgs mass cannot be reconstructed, but a transverse di–lepton mass m_T can be calculated from the lepton transverse momenta and the missing transverse energy. It is defined by $m_T^{\ell\ell} = \sqrt{2 \cdot p_T^{\ell\ell} \cdot (1 - \cos\Delta\phi(\ell\ell, \not{E}_T))}$ and should be in the range $m_H/2 < m_T < m_H - 10\,\mathrm{GeV}$ (Cut 6). Figure 8 shows the transverse mass distribution of the signal for the six different mass points. The latter two cuts further reduce backgrounds from Z/γ^* production.

- To suppress the background from $t\bar{t}$ production, the scalar sum of the transverse energies of all jets with $E_T^{\mathrm{jet}} > 20$ GeV and $|\eta| < 2.5$, H_T, is required to be less than 100 GeV (Cut 7).

- Finally, the spin correlations in the decay of the Higgs boson are used. The leptons of the Higgs decay tend to have a small opening angle, which is not expected for most of the backgrounds. Thus, it is required, that the opening angle between the leptons in the transverse plane is $\Delta\phi_{\ell\ell} < 2.0$ (Cut 8). Remaining Z boson and multi-jet events can be rejected by this cut on the opening angle since most of the background decays are back-to-back.

Table 5 summarizes the different cuts using the mass dependent selection.

	Selection criterion	Value
Cut 1	Preselection	Trigger, ID, leptons with opposite charge and $p_T^{\ell_1} > 15$ GeV and $p_T^{\ell_2} > 10$ GeV ($m_{\mu\mu} > 20\,\mathrm{GeV}$)
Cut 2	Missing transverse energy $\not{E}_T$	$\not{E}_T > 20\,\mathrm{GeV}$
Cut 3	Scaled $\not{E}_T^{\mathrm{Sc}}$	$\not{E}_T^{\mathrm{Sc}} > 15$ (for $N_{Jet} > 0$)
Cut 4	Invariant mass $m_{\ell\ell}$	$m_{\ell\ell} < m_H/2\,\mathrm{GeV}$
Cut 5	Sum of p_T and $\not{E}_T$	$m_H/2 + 20(10)\,\mathrm{GeV} < p_T^{\ell_1} + p_T^{\ell_2} + \not{E}_T < m_H$
Cut 6	Transverse mass $m_T^{\ell\ell}$	$m_H/2 < m_T^{\ell\ell} < m_H - 10\,\mathrm{GeV}$
Cut 7	H_T (scalar sum of p_T^{Jet})	$H_T^{Jet} < 100\,\mathrm{GeV}$
Cut 8	Lepton opening angle $\Delta\phi_{\ell\ell}$	$\Delta\phi_{\ell\ell} < 2.0$

Table 5: Summary of the selection criteria for a Higgs mass m_H dependent selection.

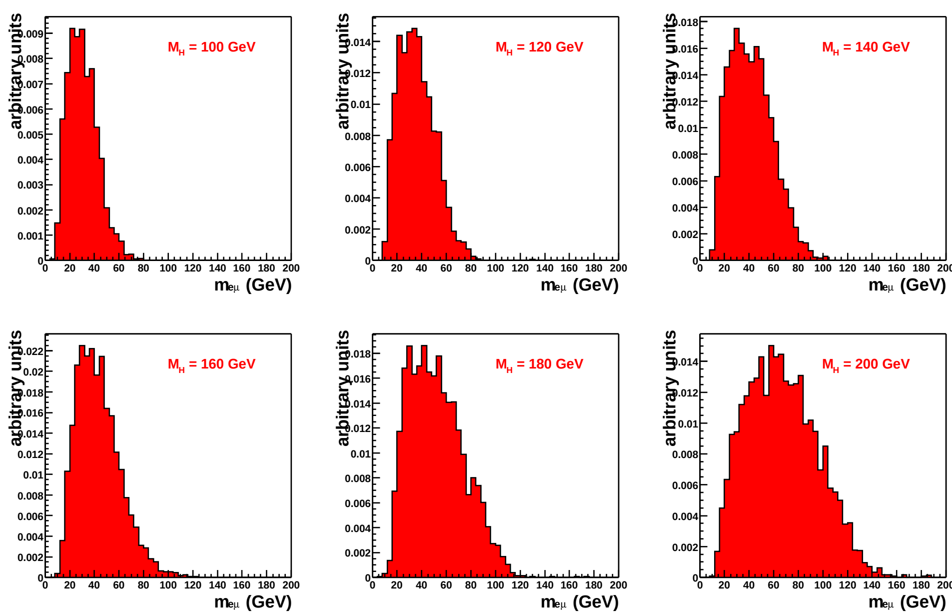

Figure 6: Distribution of the invariant mass after lepton ID, p_T and $\not{E}_T$ cuts for six different Higgs masses for the $e^{\pm}\mu^{\mp}$ final state.

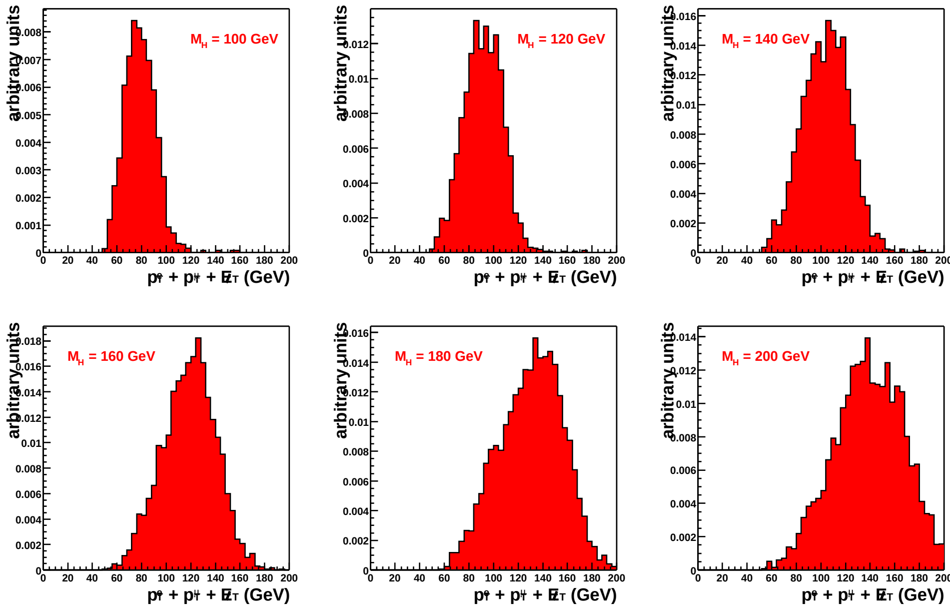

Figure 7: Distribution of the sum of the lepton transverse momentum p_T and the missing transverse momentum $\not{E}_T$ after the invariant mass cut for six different Higgs masses for the $e^{\pm}\mu^{\mp}$ final state.

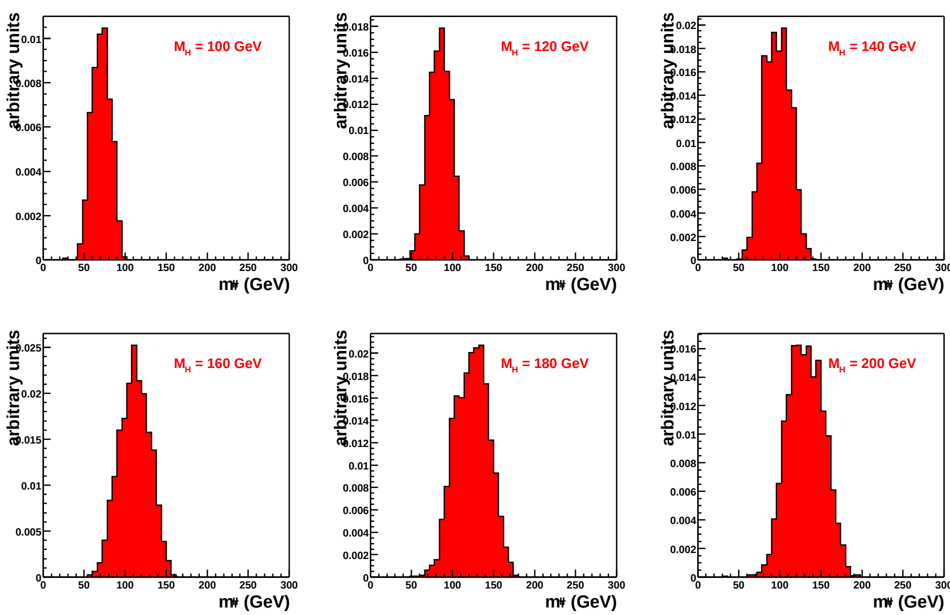

Figure 8: Distribution of the transverse mass $m_T^{\ell\ell}$ for six different Higgs masses for the $e^{\pm}\mu^{\mp}$ final state.

7.2 The e^+e^- final state

For the e^+e^- final state, events are selected based on single and di–electron triggers. Runs with failures of detector components are rejected as well as bad luminosity blocks. The total integrated luminosity for the di–electron sample is $\mathcal{L} = 325$ pb^{-1}.

Events are required to have two electrons satisfying standard electron identification criteria (isolation < 0.15, emfraction > 0.9 and HMatrix8 < 50). Furthermore the electrons must pass a likelihood criterion of 0.3.

Both electrons are required to come from the same vertex (Δz(tracks) < 2 cm) and should have opposite charge. The leading electron should have a transverse momentum of $p_T^{e_1} > 15$ GeV, the trailing electron should have a transverse momentum of $p_T^{e_2} > 10$ GeV (Cut 1). The p_T distributions for the leading and the trailing electron are shown in Fig. 9 whereas the distributions of the missing transverse energy and the scaled missing transverse energy are presented in Fig. 10.

To reject the large contribution from Z/γ^* decays, a set of cuts is applied. The missing transverse energy is required to be $\not\!\!E_T > 20$ GeV (Cut 2). Drell-Yan events can be tested if the missing transverse energy is caused by a mis-measurement of jets in the event. The scaled $\not\!\!E_T$ is required to be $\not\!\!E_T^{\text{Scaled}} > 15$ (Cut 3).

To remove remaining contributions from decays of the Z resonance, events with an invariant di–electron mass around the Z mass are rejected. Thus, only events that fulfill the condition $m_{ee} < m_H/2$ are taken further into account (Cut 4). For Higgs masses above 160 GeV, the cut is applied at 80 GeV to remove the Z peak. The invariant di–electron mass at the beginning of the selection and before the application

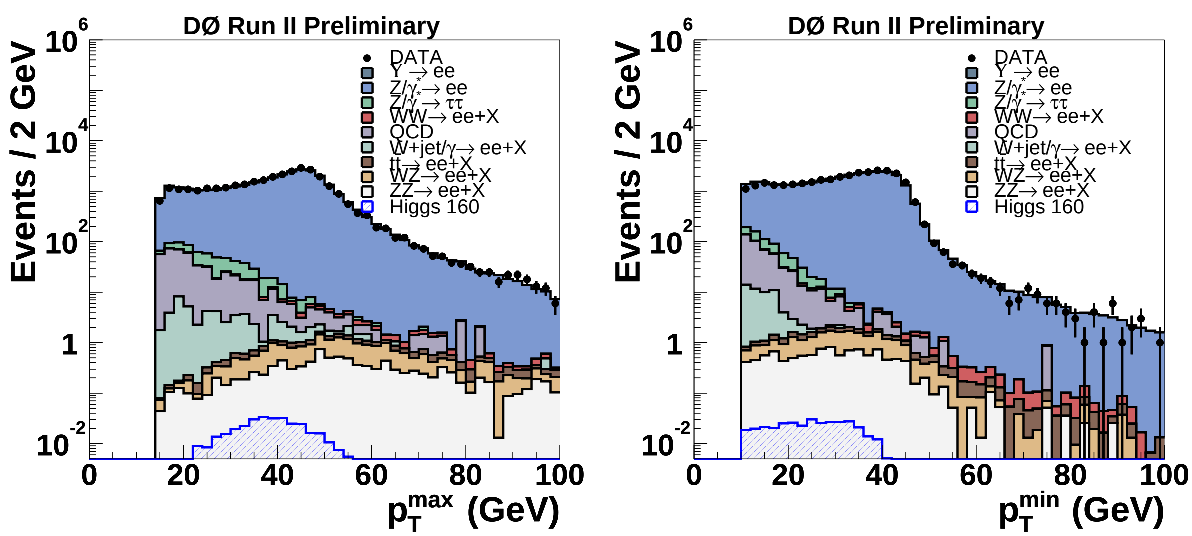

Figure 9: Distribution of the transverse momentum for the leading (left) and trailing electron (right) after the preselection (Cut 1) for the e^+e^- final state.

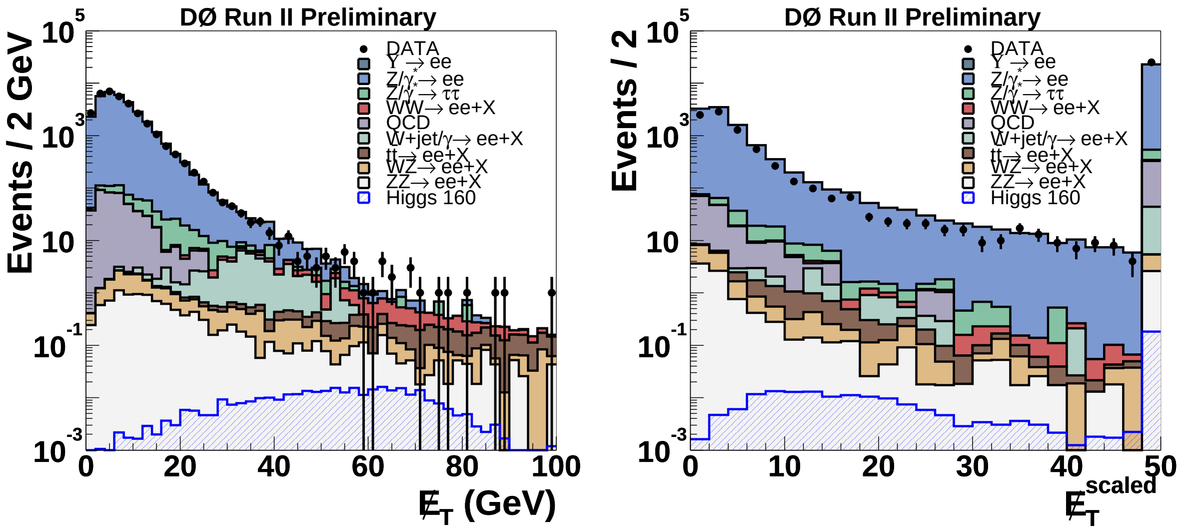

Figure 10: Distribution of the missing transverse energy $\not\!\!E_T$ (left) and of the scaled missing transverse energy $\not\!\!E_T^{\mathrm{Sc}}$ (right) after the preselection (Cut 1) for the e^+e^- final state.

of criterion 4 is presented in Fig. 11.

Drell-Yan events, that pass the invariant mass cut, can be further suppressed with a cut on the sum of the lepton transverse momenta and the missing transverse energy. The criterion is $m_H/2 + 20\,\mathrm{GeV} < p_T^{\ell_1} + p_T^{\ell_2} + \not\!\!E_T < m_H$ (Cut 5). This cut also rejects WW contributions for small Higgs masses and is expected to suppress $W + jet/\gamma$ events for large Higgs masses. The distributions after the preselection and the invariant mass cut are shown in Fig. 12.

A cut on the transverse di–lepton mass is also expected to reject remaining Drell-Yan events and a fraction of the $W + jet/\gamma$ events. A mass dependent cut of $m_H/2 < m_T^{\ell\ell} < m_H - 10\,\mathrm{GeV}$ (Cut 6) is used in the analysis. Figure 13 presents the reconstructed di–lepton mass at the preselection level and before the cut is applied.

To suppress contributions from $t\bar{t}$ events, the scalar sum of the transverse momenta of the jets is not allowed to exceed 100 GeV (Cut 7). At the end a cut on the opening angle $\Delta\phi_{ee}$ is applied at $\Delta\phi_{ee} < 2.0$ (Cut 8). The distribution of the opening angle in the transverse plane is shown in Fig. 14.

A summary of the selection criteria for the e^+e^- final state can be found in Table 6. A detailed comparison between the Monte Carlo expectation and events observed in the data after every stage of the selection is presented in Tables 7–12 for all six Higgs masses between 100 and 200 GeV.

Signal efficiencies are determined for six different Higgs masses of 100, 120, 140, 160, 180, and 200 GeV. The highest efficiencies at the beginning of the selection are obtained for heavy Higgs bosons. An efficiency of $(4.81 \pm 0.08)\%$ with respect to

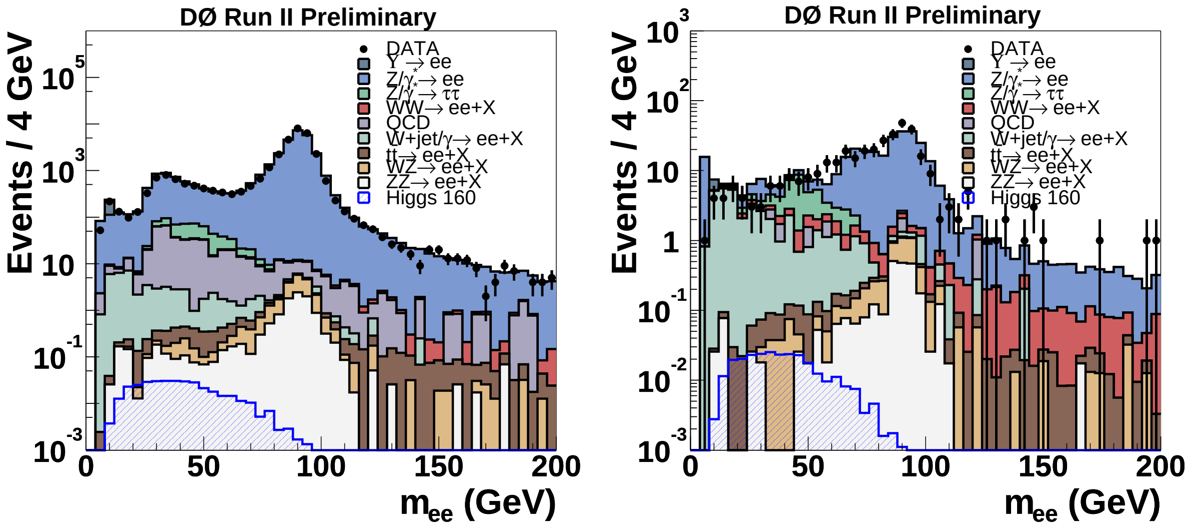

Figure 11: Distribution of the invariant mass m_{ee} after the preselection (left) and after the $\not\!\!E_T$ and $\not\!\!E_T^{\rm Sc}$ criteria are applied (right).

$H \rightarrow WW^{(*)} \rightarrow \ell^+\nu\ell'^-\bar{\nu}$ $(\ell, \ell' = e, \mu, \tau_{lep})$ decays is found for a Higgs boson of mass $m_H = 200$ GeV. Smaller efficiencies are expected for light Higgs bosons, where the efficiency after the preselection is only $(1.86 \pm 0.06)\%$ for $m_H = 100$ GeV. After the application of all cuts the selection efficiency for Higgs bosons of $m_H = 160$ GeV is $(2.14 \pm 0.06)\%$, while in the low mass region only efficiencies of $(0.56 \pm 0.03)\%$ are found. Table 13 summarizes the efficiencies for all Higgs mass and for all different steps of the selection. The number of signal events expected is 0.183 ± 0.005 for a Higgs mass of $m_H = 160$ GeV and 0.035 ± 0.001 for a Higgs mass of $m_H = 120$ GeV.

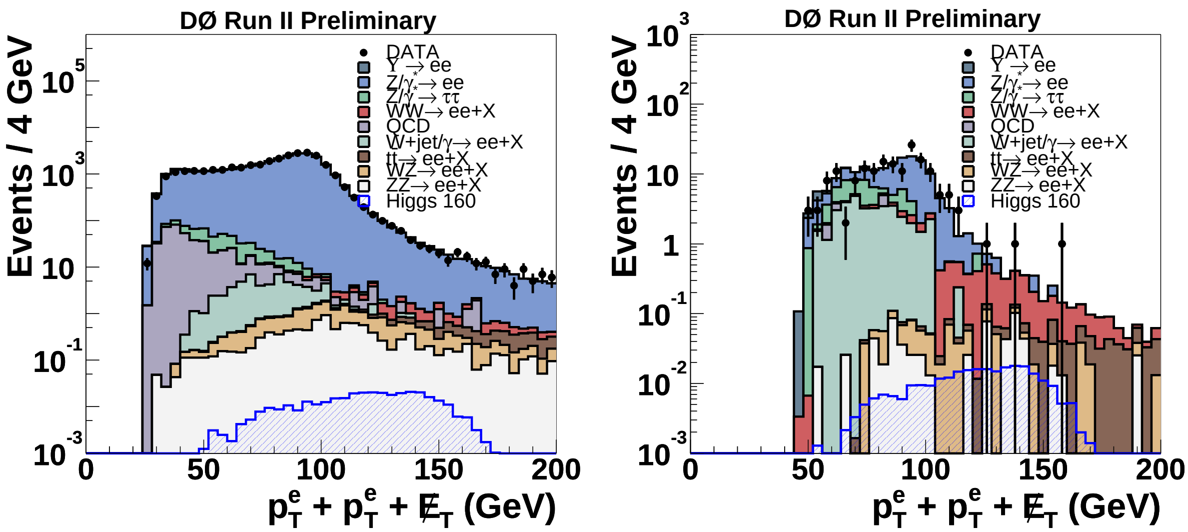

Figure 12: Distribution of the sum of the lepton transverse momenta and the missing transverse energy are shown after the preselection (left) and the invariant mass cut (right).

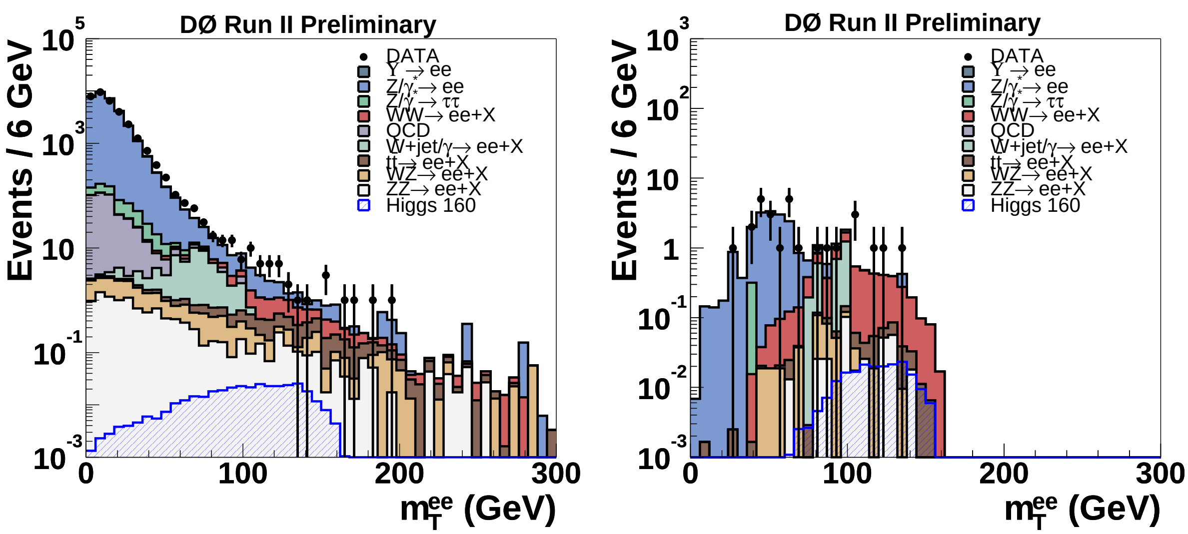

Figure 13: Distribution of the transverse di–lepton mass after the preselection (left) and before the cut on the transverse di–lepton mass (Cut 6) is applied (right).

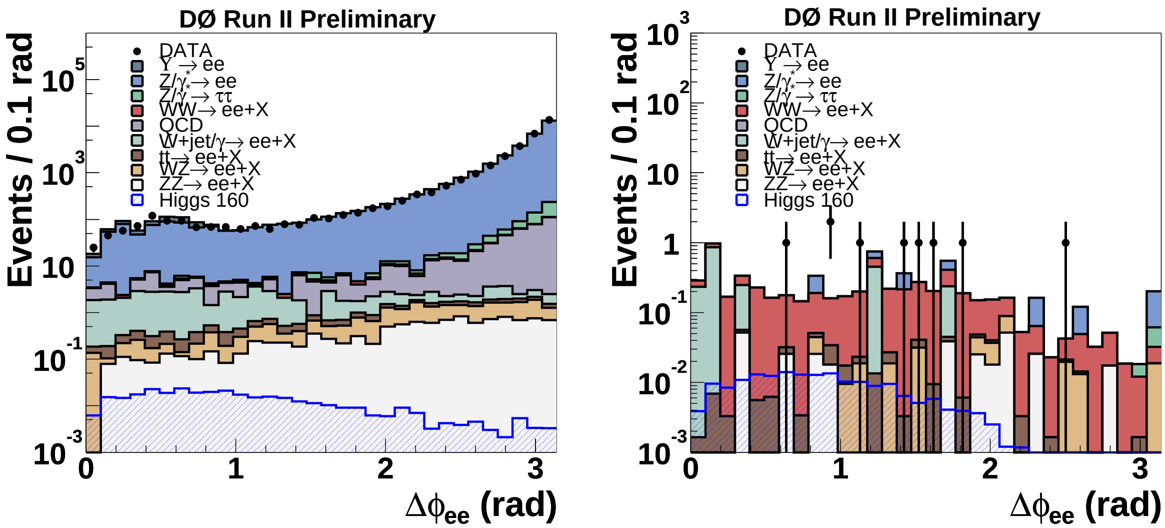

Figure 14: Distribution of the lepton opening angle in the transverse plane after the preselection (left) and before the cut on lepton opening angle (Cut 8) is applied (right) for the e^+e^- final state.

	Selection criterion	Value
Cut 1	Preselection	$p_T^{e_1} > 15$ GeV and $p_T^{e_2} > 10$ GeV and leptons with opposite charge and Δz(tracks) < 2 cm
Cut 2	Missing transverse energy	$\not\!\!E_T > 20$ GeV
Cut 3	Scaled $\not\!\!E_T$	$\not\!\!E_T^{\text{Scaled}} > 15$
Cut 4	Invariant mass	$m_{ee} < \min(m_H/2{,}80)$ GeV
Cut 5	Sum of p_T and $\not\!\!E_T$	$m_H/2 + 20\,\text{GeV} < p_T^{\ell_1} + p_T^{\ell_2} + \not\!\!E_T < m_H$
Cut 6	Transverse mass $m_T^{\ell\ell}$	$m_H/2 < m_T^{\ell\ell} < m_H - 10\,\text{GeV}$
Cut 7	Sum of jet transverse momenta	$H_T < 100$ GeV
Cut 8	Lepton opening angle $\Delta\phi_{\ell\ell}$	$\Delta\phi_{\ell\ell} < 2.0$

Table 6: Summary of the selection criteria for the e^+e^- final state.

	$t\bar{t}$	ZZ	WZ	WW	Υ
1	6.34±0.10	11.4±0.5	13.7±0.5	19.3±0.3	125±4
2	5.86±0.09	4.18±0.31	5.21±0.28	15.7±0.3	4.78±0.79
3	1.47±0.05	2.58±0.24	3.21±0.22	13.6±0.3	2.54±0.60
4	0.37±0.02	0.17±0.07	0.17±0.05	3.95±0.16	0.87±0.35
5	0.01±0.01	0.04±0.03	0.09±0.04	1.48±0.10	0.0±0.0
6	0.01±0.01	0.02±0.02	0.06±0.03	1.15±0.08	0.0±0.0
7	0.01±0.01	0.02±0.02	0.06±0.03	1.15±0.08	0.0±0.0
8	0.01±0.01	0.02±0.02	0.0±0.0	1.00±0.08	0.0±0.0

	$Z/\gamma^* \to \tau\tau$	$Z/\gamma^* \to ee$	$W + jet/\gamma$	QCD	Sum	Data
1	270±9	32294±53	48.0±4.1	428±18	33216± 57 ±2159	33018
2	53.4±4.0	827±8	43.4±3.9	12.0±3.0	972± 10 ±63	964
3	27.6±2.8	279±5	38.9±3.7	4.50±1.84	373± 7 ±24	367
4	11.0±2.0	11.7±1.6	20.1±2.9	1.50±1.06	49.8±4.0±3.24	58
5	6.47±1.49	4.86±1.04	10.5±2.0	0.75±0.75	24.3±2.8±1.6	22
6	0.93±0.42	1.69±0.64	10.4±2.0	0.75±0.75	15.0±2.2±1.0	17
7	0.93±0.42	1.69±0.64	10.4±2.0	0.75±0.75	15.0±2.2±1.0	17
8	0.0±0.0	0.97±0.48	9.06±1.85	0.0±0.0	11.1±1.9±0.72	11

Table 7: Number of background events expected, and number of events observed, after successive selections for an integrated luminosity of $\int \mathcal{L}dt = 325$ pb^{-1} in the e^+e^- channel for the m_H=100 GeV selection. The statistical error is listed for all backgrounds. The systematical error described in Section 8 without the uncertainty of the integrated luminosity is only given for the sum of all backgrounds.

	$t\bar{t}$	ZZ	WZ	WW	Υ
1	6.34±0.10	11.4±0.5	13.7±0.5	19.3±0.3	125±4
2	5.86±0.09	4.18±0.31	5.21±0.28	15.7±0.3	4.78±0.79
3	1.47±0.05	2.58±0.24	3.21±0.22	13.6±0.3	2.54±0.60
4	0.54±0.03	0.26±0.08	0.24±0.06	5.92±0.19	2.54±0.60
5	0.05±0.01	0.07±0.04	0.16±0.05	2.83±0.13	0.0±0.0
6	0.04±0.01	0.07±0.04	0.09±0.04	2.46±0.12	0.0±0.0
7	0.03±0.01	0.07±0.04	0.09±0.04	2.46±0.12	0.0±0.0
8	0.03±0.01	0.07±0.04	0.04±0.03	2.10±0.11	0.0±0.0

	$Z/\gamma^* \to \tau\tau$	$Z/\gamma^* \to ee$	$W + jet/\gamma$	QCD	Sum	Data
1	270±9	32294±53	48.0±4.1	428±18	33216± 57 ±2159	33018
2	53.4±4.0	827±8	43.4±3.9	12.0±3.0	972± 10 ±63	964
3	27.6±2.8	279±5	38.9±3.7	4.50±1.84	373± 7 ±24	367
4	24.1±2.8	21.4±2.1	32.3±3.5	3.00±1.50	90.3±5.3±5.9	82
5	3.47±0.93	4.07±0.83	11.7±2.0	1.50±1.06	23.8±2.6±1.6	25
6	1.81±0.68	0.90±0.40	11.5±2.0	0.0±0.0	16.8±2.2±1.1	16
7	1.81±0.68	0.90±0.40	11.5±2.0	0.0±0.0	16.8±2.2±1.1	16
8	0.0±0.0	0.42±0.24	9.50±1.86	0.0±0.0	12.1±1.9±0.8	9

Table 8: Number of background events expected, and number of events observed, after successive selections for an integrated luminosity of $\int \mathcal{L}\mathrm{d}t = 325\ \mathrm{pb}^{-1}$ in the e^+e^- channel for the m_H=120 GeV selection. The statistical error is listed for all backgrounds. The systematical error described in Section 8 without the uncertainty of the integrated luminosity is only given for the sum of all backgrounds.

	$t\bar{t}$	ZZ	WZ	WW	Υ
1	6.34±0.10	11.4±0.5	13.7±0.5	19.3±0.3	125±4
2	5.86±0.09	4.18±0.31	5.21±0.28	15.7±0.3	4.78±0.79
3	1.47±0.05	2.58±0.24	3.21±0.22	13.6±0.3	2.54±0.60
4	0.68±0.03	0.43±0.10	0.40±0.08	7.27±0.21	2.54±0.60
5	0.13±0.01	0.24±0.07	0.22±0.06	4.12±0.16	0.0±0.0
6	0.11±0.01	0.17±0.07	0.14±0.05	3.47±0.15	0.0±0.0
7	0.07±0.01	0.17±0.07	0.14±0.05	3.47±0.15	0.0±0.0
8	0.06±0.01	0.15±0.06	0.09±0.04	3.05±0.14	0.0±0.0

	$Z/\gamma^* \to \tau\tau$	$Z/\gamma^* \to ee$	$W + jet/\gamma$	QCD	Sum	Data
1	270±9	32294±53	48.0±4.1	428±18	33216± 57 ±2159	33018
2	53.4±4.0	827±8	43.4±3.9	12.0±3.0	972± 10 ±63	964
3	27.6±2.8	279±5	38.9±3.7	4.50±1.84	373± 7 ±24	367
4	27.1±2.9	48.4±2.7	34.7±3.6	3.00±1.50	125± 6 ±8	122
5	3.57±0.87	14.0±1.3	6.23±1.25	0.0±0.0	28.5± 2.0 ±1.9	34
6	0.04±0.02	0.77±0.31	4.55±1.07	0.0±0.0	9.25±1.13±0.60	12
7	0.04±0.02	0.77±0.31	4.55±1.07	0.0±0.0	9.21±1.13±0.60	12
8	0.0±0.0	0.39±0.23	3.60±0.96	0.0±0.0	7.34±1.00±0.48	10

Table 9: Number of background events expected, and number of events observed, after successive selections for an integrated luminosity of $\int \mathcal{L}dt = 325$ pb^{-1} in the e^+e^- channel for the m_H=140 GeV selection. The statistical error is listed for all backgrounds. The systematical error described in Section 8 without the uncertainty of the integrated luminosity is only given for the sum of all backgrounds.

	$t\bar{t}$	ZZ	WZ	WW	Υ
1	6.34±0.10	11.4±0.5	13.7±0.5	19.3±0.3	125±4
2	5.86±0.09	4.18±0.31	5.21±0.28	15.7±0.3	4.78±0.79
3	1.47±0.05	2.58±0.24	3.21±0.22	13.6±0.3	2.54±0.60
4	0.77±0.03	0.67±0.12	0.68±0.11	8.40±0.23	2.54±0.60
5	0.28±0.02	0.34±0.09	0.35±0.08	4.29±0.16	0.0±0.0
6	0.24±0.02	0.30±0.08	0.22±0.06	3.58±0.15	0.0±0.0
7	0.15±0.02	0.30±0.08	0.22±0.06	3.58±0.15	0.0±0.0
8	0.13±0.01	0.19±0.07	0.12±0.04	3.17±0.14	0.0±0.0

	$Z/\gamma^* \to \tau\tau$	$Z/\gamma^* \to ee$	$W + jet/\gamma$	QCD	Sum	Data
1	270±9	32294±53	48.0±4.1	428±18	33216± 57 ±2159	33018
2	53.4±4.0	827±8	43.4±3.9	12.0±3.0	972± 10 ±63	964
3	27.6±2.8	279±5	38.9±3.7	4.50±1.84	373± 7 ±24	367
4	27.4±2.9	93.9±3.6	35.7±3.6	3.00±1.50	173± 6 ±11	168
5	0.34±0.12	16.9±1.4	2.39±0.85	0.0±0.0	24.9± 1.7 ±1.6	27
6	0.04±0.01	0.89±0.34	1.91±0.78	0.0±0.0	7.17±0.87±0.47	9
7	0.04±0.01	0.89±0.34	1.91±0.78	0.0±0.0	7.08±0.87±0.46	9
8	0.0±0.0	0.58±0.29	1.91±0.78	0.0±0.0	6.10±0.85±0.40	8

Table 10: Number of background events expected, and number of events observed, after successive selections for an integrated luminosity of $\int \mathcal{L}dt = 325$ pb^{-1} in the e^+e^- channel for the m_H=160 GeV selection. The statistical error is listed for all backgrounds. The systematical error described in Section 8 without the uncertainty of the integrated luminosity is only given for the sum of all backgrounds.

	$t\bar{t}$	ZZ	WZ	WW	Υ
1	6.34±0.10	11.4±0.5	13.7±0.5	19.3±0.3	125±4
2	5.86±0.09	4.18±0.31	5.21±0.28	15.7±0.3	4.78±0.79
3	1.47±0.05	2.58±0.24	3.21±0.22	13.6±0.3	2.54±0.60
4	0.77±0.03	0.67±0.12	0.68±0.11	8.40±0.23	2.54±0.60
5	0.43±0.03	0.32±0.09	0.34±0.08	3.48±0.15	0.0±0.0
6	0.38±0.02	0.27±0.08	0.15±0.05	3.07±0.14	0.0±0.0
7	0.22±0.02	0.27±0.08	0.15±0.05	3.07±0.14	0.0±0.0
8	0.20±0.02	0.19±0.07	0.08±0.04	2.78±0.13	0.0±0.0

	$Z/\gamma^* \to \tau\tau$	$Z/\gamma^* \to ee$	$W + jet/\gamma$	QCD	Sum	Data
1	270±9	32294±53	48.0±4.1	428±18	33216± 57 ±2159	33018
2	53.4±4.0	827±8	43.4±3.9	12.0±3.0	972± 10 ±63	964
3	27.6±2.8	279±5	38.9±3.7	4.50±1.84	373± 7 ±24	367
4	27.4±2.9	93.9±3.6	35.7±3.6	3.00±1.50	173± 6.1 ±11	168
5	0.33±0.13	3.95±0.69	0.19±0.19	0.0±0.0	9.04±0.75±0.59	8
6	0.02±0.01	0.43±0.25	0.0±0.0	0.0±0.0	4.33±0.30±0.28	6
7	0.02±0.01	0.43±0.25	0.0±0.0	0.0±0.0	4.17±0.30±0.27	6
8	0.0±0.0	0.43±0.25	0.0±0.0	0.0±0.0	3.68±0.29±0.24	6

Table 11: Number of background events expected, and number of events observed, after successive selections for an integrated luminosity of $\int \mathcal{L}dt = 325$ pb^{-1} in the e^+e^- channel for the m_H=180 GeV selection. The statistical error is listed for all backgrounds. The systematical error described in Section 8 without the uncertainty of the integrated luminosity is only given for the sum of all backgrounds.

	$t\bar{t}$	ZZ	WZ	WW	Υ
1	6.34±0.10	11.4±0.5	13.7±0.5	19.3±0.3	125±4
2	5.86±0.09	4.18±0.31	5.21±0.28	15.7±0.3	4.78±0.79
3	1.47±0.05	2.58±0.24	3.21±0.22	13.6±0.3	2.54±0.60
4	0.77±0.03	0.67±0.12	0.68±0.11	8.40±0.23	2.54±0.60
5	0.56±0.03	0.32±0.09	0.24±0.06	2.74±0.13	0.0±0.0
6	0.50±0.03	0.19±0.06	0.11±0.04	2.46±0.13	0.0±0.0
7	0.25±0.02	0.19±0.06	0.11±0.04	2.46±0.13	0.0±0.0
8	0.23±0.02	0.16±0.06	0.07±0.03	2.26±0.12	0.0±0.0

	$Z/\gamma^* \to \tau\tau$	$Z/\gamma^* \to ee$	$W + jet/\gamma$	QCD	Sum	Data
1	270±9	32294±53	48.0±4.1	428±18	33216± 57 ±2159	33018
2	53.4±4.0	827±8	43.4±3.88	12.0±3.0	972± 10 ±63	964
3	27.6±2.8	279±5	38.9±3.66	4.50±1.84	373± 7 ±24	367
4	27.4±2.9	93.9±3.6	35.7±3.6	3.00±1.50	173± 6 ±11	168
5	0.32±0.16	0.96±0.34	0.0±0.0	0.0±0.0	5.13±0.41±0.33	3
6	0.01±0.01	0.15±0.15	0.0±0.0	0.0±0.0	3.42±0.21±0.22	3
7	0.01±0.01	0.15±0.15	0.0±0.0	0.0±0.0	3.18±0.21±0.21	3
8	0.0±0.0	0.15±0.15	0.0±0.0	0.0±0.0	2.87±0.20±0.19	3

Table 12: Number of background events expected, and number of events observed, after successive selections for an integrated luminosity of $\int \mathcal{L}dt = 325$ pb^{-1} in the e^+e^- channel for the m_H=200 GeV selection. The statistical error is listed for all backgrounds. The systematical error described in Section 8 without the uncertainty of the integrated luminosity is only given for the sum of all backgrounds.

m_H	100	120	140	160	180	200
			Signal Efficiencies (%)			
1	1.86±0.06	3.03±0.07	3.77±0.09	4.23±0.09	4.74±0.09	4.81±0.08
2	1.50±0.05	2.69±0.06	3.42±0.08	4.01±0.09	4.46±0.09	4.50±0.08
3	1.14±0.04	2.12±0.06	2.71±0.07	3.30±0.08	3.63±0.08	3.60±0.07
4	1.05±0.04	2.02±0.05	2.53±0.07	3.22±0.08	3.21±0.07	2.65±0.06
5	0.73±0.04	1.47±0.05	1.85±0.06	2.40±0.07	2.33±0.06	1.79±0.05
6	0.62±0.03	1.34±0.04	1.67±0.06	2.21±0.06	2.20±0.06	1.67±0.05
7	0.61±0.03	1.34±0.04	1.67±0.06	2.21±0.06	2.17±0.06	1.62±0.05
8	0.56±0.03	1.18±0.04	1.55±0.06	2.14±0.06	2.12±0.06	1.57±0.05
Exp. Events	0.002±0.001	0.035±0.001	0.107±0.004	0.183±0.005	0.128±0.004	0.053±0.002

Table 13: Efficiencies in % with respect to $H \to WW^{(*)} \to \ell^+\nu\ell'^-\bar{\nu}$ $(\ell, \ell' = e, \mu, \tau_{lep})$ decays for the Higgs signal for six different Higgs masses between 100 and 200 GeV for the different stages of the selection and number of events expected for a standard model Higgs boson at the end of the selection for the e^+e^- final state. Only statistical uncertainties are given.

7.3 The $e^{\pm}\mu^{\mp}$ final state

Starting from the EMMU skim, events are selected with the following criteria. The events must be triggered by an electron–muon trigger. Again runs with hardware failures and bad luminosity blocks are rejected resulting in a data sample corresponding to $\mathcal{L} = 318$ pb^{-1}. The events must have at least one electron matching the electron identification criteria and $p_T > 15$ GeV. Furthermore one muon satisfying loose muon identification criteria with $p_T > 10$ GeV is required.

Both leptons should come from the same vertex (Δz(tracks) < 2 cm) and are required to have opposite charge (Cut 1, Table 14). This leaves 755 events in the data. The p_T distributions of the leading and the trailing lepton for these events are shown in Fig. 15 whereas the distribution of the missing transverse energy is presented in Fig. 16 (left).

After the implementation of the lepton identification and kinematic criteria, the dominant background in the selected sample is from $Z/\gamma^* \to \tau\tau$ decays. Other background sources are $W + jet/\gamma$ events, where either the jet fakes an electron or the W boson radiates a photon that converts into an electron–positron pair, and multi–jet production. No significant $\not\!\!E_T$ is expected from the latter. Remaining contributions from $Z/\gamma^* \to \mu\mu$ decays and also a fraction of the $Z/\gamma^* \to \tau\tau$ events can be rejected by requiring $\not\!\!E_T > 20$ GeV (Cut 2). To further reduce the Z/γ^* contribution a cut on the scaled missing transverse energy is applied: $\not\!\!E_T^{\text{Scaled}} > 15$ (Cut 3). The distribution of the scaled missing transverse energy is presented in Fig. 16 (right).

The invariant mass $m_{e\mu}$, which is shown in Fig. 17 (left) after the preselection and in Fig. 17 (right) before the implementation of the criterion, is restricted to $m_H/2$ for the signal. Thus the invariant mass is required to be $m_{e\mu} < m_H/2$ (Cut 4).

A mass dependent cut for the sum of the lepton transverse momenta and the missing transverse energy is applied. The following cut is applied: $m_H/2 + 20\,\text{GeV} < p_T^{\ell_1} + p_T^{\ell_2} + \not\!\!E_T < m_H$ (Cut 5). For small Higgs masses, this cut reduces a large fraction of WW events which are expected to have large values for the lepton transverse momenta and the missing transverse energy. On the other hand, for large Higgs masses, this cut rejects $W + jet$ and $W + \gamma$ events, since for both event types, the p_T of the fake electron is expected to be small. The distribution at the preselection stage is presented in Fig. 18 (left), whereas in Fig. 18 (right) the distribution is shown before the cut is applied.

The distribution of the di–lepton transverse mass m_T after the preselection is shown in Fig. 19 (left). Requiring $m_H/2 < m_T^{\ell\ell} < m_H - 10\,\text{GeV}$ (Cut 6) rejects remaining Z/γ and multi-jet events. Figure 19 (right) presents the distribution before the application of the criterion.

A cut on the sum of the jet transverse momenta, $H_T < 100$ GeV (Cut 7), is used to reject a fraction of remaining $t\bar{t}$ events. To remove remaining Z and multi-jet events a cut on the opening angle of the two leptons in the transverse plane is applied at $\Delta\phi_{e\mu} <$

2.0 (Cut 8). The distribution of the opening angle after the preselection is shown in Fig. 20 (left). The corresponding distribution before application of the criterion can be seen in Fig. 20 (right). A summary of all the selection criteria can be found in Table 14.

A detailed comparison between the Monte Carlo expectation and events observed in the data after every stage of the selection is presented in Tables 15–20 for all six Higgs masses between 100 and 200 GeV.

The signal efficiencies are determined for the six different Higgs masses of 100, 120, 140, 160, 180, and 200 GeV. At the beginning of the selection, the efficiencies are the highest for heavy Higgs bosons. The efficiency is $(10.61 \pm 0.13)\%$ with respect to $H \to WW^{(*)} \to \ell^+\nu\ell'^-\bar{\nu}$ $(\ell, \ell' = e, \mu, \tau_{lep})$ decays for a Higgs boson of mass $m_H = 200$ GeV. Smaller efficiencies are expected for light Higgs bosons, where the efficiency after the preselection is only $(3.47 \pm 0.08)\%$ for $m_H = 100$ GeV. After the final selection, the selection efficiency for Higgs bosons between 160 and 180 GeV is $(3.92 \pm 0.09)\%$, while in the low mass region only efficiencies of $(1.02 \pm 0.04)\%$ are expected. Table 21 summarizes the efficiencies for all Higgs mass and for all different steps of the selection. Using these efficiencies and the cross sections from Table 3, 0.355 ± 0.008 Higgs events are expected for a Higgs mass of $m_H = 160$ GeV and 0.064 ± 0.002 Higgs events for a Higgs mass of $m_H = 120$ GeV.

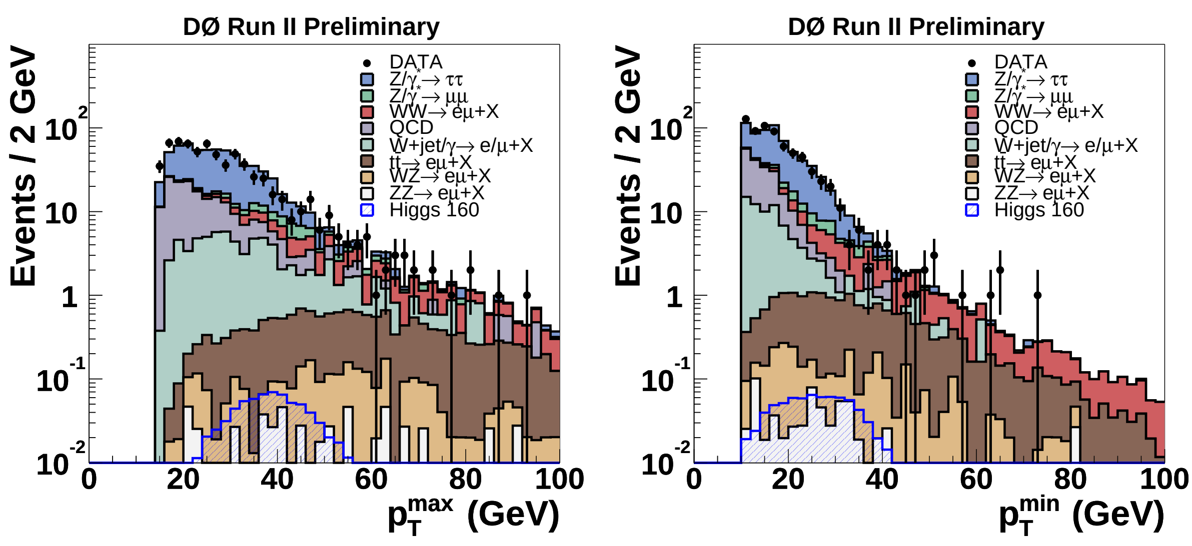

Figure 15: Distribution of the transverse momentum of the leading (left) and trailing lepton (right) after the preselection (Cut 1) for the $e^{\pm}\mu^{\mp}$ final state.

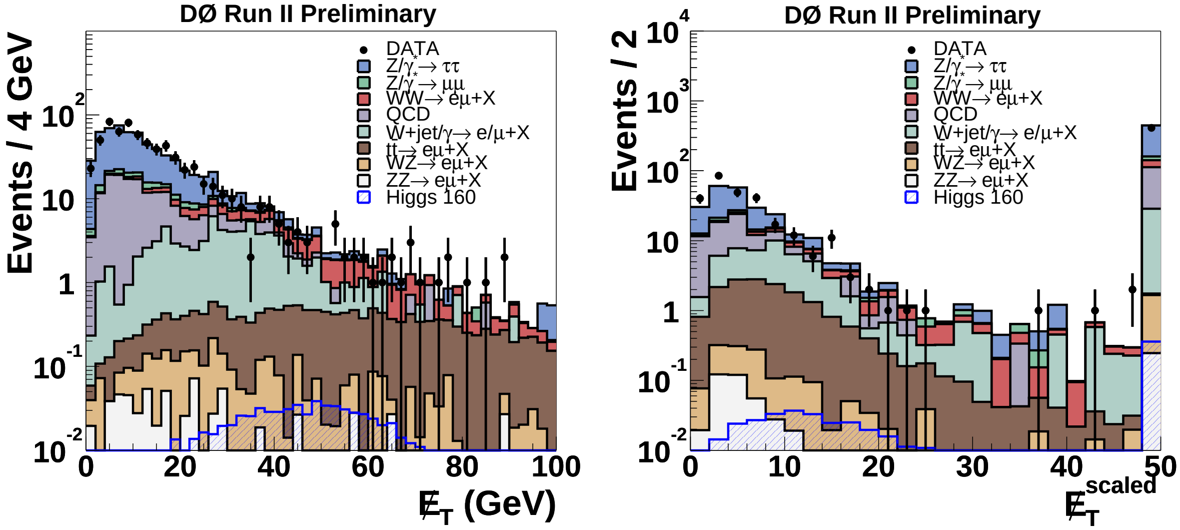

Figure 16: Distribution of the missing transverse energy $\not\!\!E_T$ (left) and scaled missing transverse energy (right) after the preselection (Cut 1) for the $e^{\pm}\mu^{\mp}$ final state.

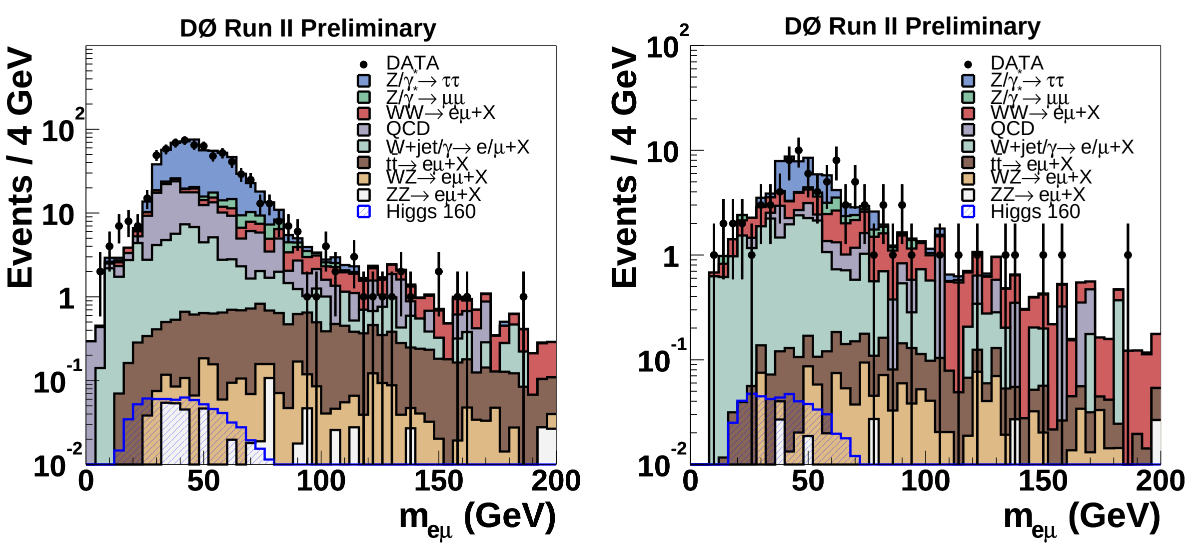

Figure 17: Distribution of the invariant di–lepton mass after the preselection (left) and before the cut on the invariant di–lepton mass (Cut 4) is applied (right) for the $e^{\pm}\mu^{\mp}$ channel.

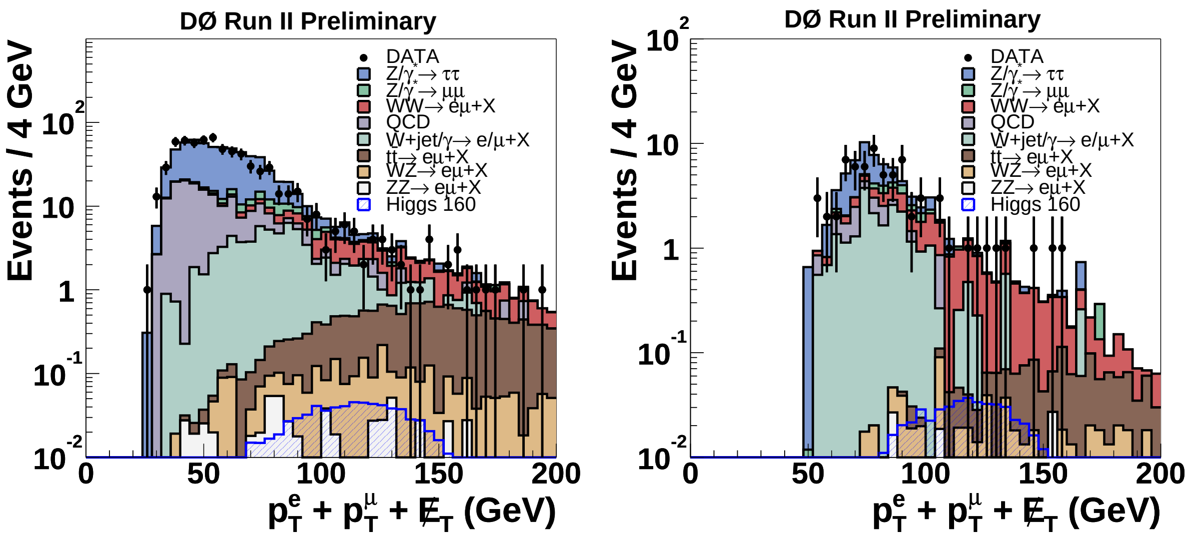

Figure 18: Distribution of the sum of the lepton transverse momenta and the missing transverse energy after the preselection (left) and before the cut on this sum (Cut 5) is applied (right) for the $e^{\pm}\mu^{\mp}$ channel.

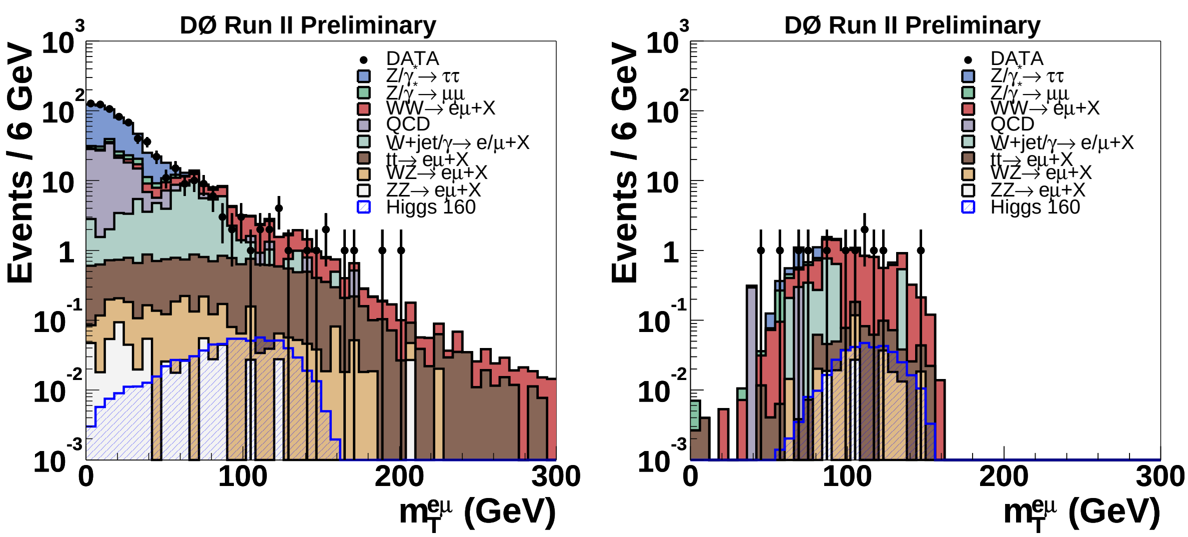

Figure 19: Distribution of the transverse di–lepton mass $m_T^{\ell\ell}$ after the preselection (left) and before the cut on the transverse di–lepton mass (Cut 6) is applied (right) for the $e^{\pm}\mu^{\mp}$ channel.

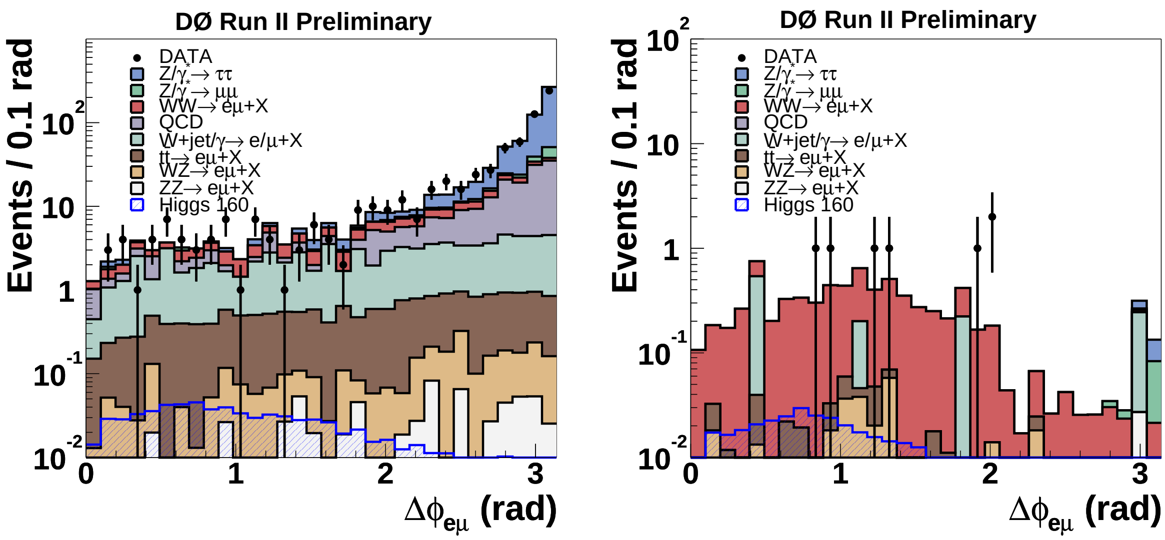

Figure 20: Distribution of the opening angle in the transverse plane $\Delta\phi_{e\mu}$ after the preselection (left) and before the cut opening angle (Cut 8) is applied (right) for the $e^{\pm}\mu^{\mp}$ channel.

	Selection criterion	Value
Cut 1	Preselection	$p_T^{e_1} > 15$ GeV and $p_T^{e_2} > 10$ GeV and leptons with opposite charge and Δz(tracks) < 2 cm
Cut 2	Missing transverse energy	$\not\!\!E_T > 20$ GeV
Cut 3	Scaled $\not\!\!E_T$	$\not\!\!E_T^{\mathrm{Scaled}} > 15$
Cut 4	Invariant mass	$m_{e\mu} < m_H/2$
Cut 5	Sum of p_T and $\not\!\!E_T$	$m_H/2 + 20\,\mathrm{GeV} < p_T^{\ell_1} + p_T^{\ell_2} + \not\!\!E_T < m_H$
Cut 6	Transverse mass $m_T^{\ell\ell}$	$m_H/2 < m_T^{\ell\ell} < m_H - 10\,\mathrm{GeV}$
Cut 7	Sum of jet transverse momenta	$H_T < 100$ GeV
Cut 8	Lepton opening angle $\Delta\phi_{\ell\ell}$	$\Delta\phi_{\ell\ell} < 2.0$

Table 14: Summary of the selection criteria for the $e^{\pm}\mu^{\mp}$ final state.

	$t\bar{t}$	ZZ	WZ	WW
1	15.9±0.2	0.61±0.12	2.69±0.22	42.7±0.5
2	14.4±0.2	0.31±0.09	2.03±0.19	32.7±0.5
3	2.59±0.10	0.13±0.06	1.44±0.16	27.1±0.4
4	0.59±0.05	0.05±0.03	0.18±0.06	7.88±0.23
5	0.02±0.01	0.03±0.03	0.06±0.03	3.32±0.15
6	0.02±0.01	0.03±0.03	0.04±0.03	2.46±0.13
7	0.02±0.01	0.03±0.03	0.04±0.03	2.46±0.13
8	0.02±0.01	0.03±0.03	0.04±0.03	2.31±0.13

	$Z/\gamma^* \to \mu\mu$	$Z/\gamma^* \to \tau\tau$	$W + jet/\gamma$	QCD	Sum	Data
1	26.5±0.6	409±10	66.3±3.8	124±6	688± 13 ±45	691
2	7.31±0.28	65.6±4.0	49.0±3.2	23.1±2.5	195± 6 ±13	174
3	4.75±0.24	26.1±2.4	25.8±2.4	9.84±1.62	97.8±3.8±6.4	90
4	0.82±0.12	16.5±2.2	15.4±1.8	2.93±0.88	44.3±3.0±2.9	39
5	0.59±0.11	8.65±1.64	10.4±1.4	1.06±0.53	24.1±2.2±1.6	20
6	0.29±0.10	0.33±0.33	8.90±1.34	0.27±0.27	12.3±1.4±0.8	13
7	0.29±0.10	0.33±0.33	8.90±1.34	0.27±0.27	12.3±1.4±0.8	13
8	0.26±0.19	0.0±0.0	7.88±1.26	0.27±0.27	10.8±1.3±0.7	12

Table 15: Number of background events expected, and number of events observed, after successive selections for an integrated luminosity of $\int \mathcal{L}dt = 318$ pb^{-1} in the $e^{\pm}\mu^{\mp}$ channel for the m_H=100 GeV selection. The statistical error is listed for all backgrounds. The systematical error described in Section 8 without the uncertainty of the integrated luminosity is only given for the sum of all backgrounds.

	$t\bar{t}$	ZZ	WZ	WW
1	15.9±0.2	0.61±0.12	2.69±0.22	42.7±0.5
2	14.4±0.2	0.31±0.09	2.03±0.19	32.7±0.5
3	2.59±0.10	0.13±0.06	1.44±0.16	27.1±0.4
4	0.79±0.05	0.05±0.03	0.27±0.07	10.7±0.3
5	0.11±0.02	0.05±0.03	0.12±0.05	5.81±0.20
6	0.09±0.02	0.02±0.02	0.10±0.04	4.29±0.17
7	0.07±0.02	0.02±0.02	0.10±0.04	4.28±0.17
8	0.06±0.02	0.00±0.00	0.08±0.04	4.07±0.17

	$Z/\gamma^* \to \mu\mu$	$Z/\gamma^* \to \tau\tau$	$W + jet/\gamma$	QCD	Sum	Data
1	26.5±0.6	409±10	66.3±3.9	124±6	688± 13 ±45	691
2	7.31±0.28	65.6±4.0	49.0±3.2	23.1±2.5	195± 6 ±13	174
3	4.75±0.24	26.1±2.4	25.8±2.4	9.84±1.62	97.8± 3.8 ±6.4	90
4	1.92±0.18	22.6±2.4	19.2±2.0	3.72±1.00	59.2± 3.4 ±3.9	51
5	1.25±0.15	4.52±1.13	8.21±1.28	0.80±0.46	20.9± 1.8 ±1.4	13
6	0.33±0.08	0.57±0.40	5.43±1.01	0.27±0.27	11.1± 1.1 ±0.7	5
7	0.33±0.08	0.57±0.40	5.43±1.01	0.27±0.27	11.1± 1.1 ±0.7	5
8	0.26±0.19	0.0±0.0	4.68±0.94	0.00±0.00	9.16±0.97±0.60	5

Table 16: Number of background events expected, and number of events observed, after successive selections for an integrated luminosity of $\int \mathcal{L}dt = 318$ pb^{-1} in the $e^{\pm}\mu^{\mp}$ channel for the m_H=120 GeV selection. The statistical error is listed for all backgrounds. The systematical error described in Section 8 without the uncertainty of the integrated luminosity is only given for the sum of all backgrounds.

	$t\bar{t}$	ZZ	WZ	WW
1	15.9±0.2	0.61±0.12	2.69±0.22	42.7±0.5
2	14.4±0.2	0.31±0.09	2.03±0.19	32.7±0.5
3	2.59±0.10	0.13±0.06	1.44±0.16	27.1±0.4
4	1.04±0.06	0.05±0.03	0.41±0.09	13.5±0.3
5	0.28±0.03	0.02±0.02	0.18±0.06	7.30±0.22
6	0.24±0.03	0.02±0.02	0.09±0.04	5.56±0.19
7	0.14±0.02	0.02±0.02	0.09±0.04	5.54±0.19
8	0.14±0.02	0.0±0.0	0.08±0.04	5.26±0.19

	$Z/\gamma^* \to \mu\mu$	$Z/\gamma^* \to \tau\tau$	$W + jet/\gamma$	QCD	Sum	Data
1	26.5±0.6	409±10	66.3±3.8	124±6	688± 13 ±45	691
2	7.31±0.28	65.6±4.0	49.0±3.2	23.1±2.5	195± 6 ±13	174
3	4.75±0.24	26.1±2.4	25.8±2.4	9.84±1.62	97.8± 3.8 ±6.4	90
4	3.20±0.24	24.3±2.4	20.5±2.1	5.05±1.16	68.0± 3.5 ±4.4	66
5	0.77±0.09	1.73±0.61	5.33±1.03	0.53±0.38	16.1± 1.3 ±1.1	13
6	0.08±0.02	0.39±0.27	3.16±0.77	0.0±0.0	9.53±0.84±0.62	4
7	0.08±0.02	0.39±0.27	3.16±0.77	0.0±0.0	9.42±0.84±0.61	4
8	0.0±0.0	0.0±0.0	2.17±0.63	0.0±0.0	7.64±0.65±0.50	4

Table 17: Number of background events expected, and number of events observed, after successive selections for an integrated luminosity of $\int \mathcal{L}dt = 318$ pb^{-1} in the $e^{\pm}\mu^{\mp}$ channel for the m_H=140 GeV selection. The statistical error is listed for all backgrounds. The systematical error described in Section 8 without the uncertainty of the integrated luminosity is only given for the sum of all backgrounds.

	$t\bar{t}$	ZZ	WZ	WW
1	15.9±0.2	0.61±0.12	2.69±0.22	42.7±0.5
2	14.4±0.2	0.31±0.09	2.03±0.19	32.7±0.5
3	2.59±0.10	0.13±0.06	1.44±0.16	27.1±0.4
4	1.24±0.07	0.07±0.04	0.54±0.10	16.0±0.3
5	0.60±0.05	0.05±0.03	0.27±0.07	8.03±0.23
6	0.47±0.04	0.03±0.03	0.23±0.06	5.90±0.20
7	0.27±0.03	0.03±0.03	0.23±0.06	5.89±0.20
8	0.25±0.03	0.0±0.0	0.20±0.06	5.51±0.19

	$Z/\gamma^* \to \mu\mu$	$Z/\gamma^* \to \tau\tau$	$W + jet/\gamma$	QCD	Sum	Data
1	26.5±0.6	409.±10.39	66.3±3.8	124±6	688± 13 ±45	691
2	7.31±0.28	65.6±4.0	49.0±3.2	23.1±2.5	195± 6 ±13	174
3	4.75±0.24	26.1±2.4	25.8±2.4	9.84±1.62	97.8± 3.8 ±6.4	90
4	3.82±0.24	25.4±2.4	22.0±2.2	5.58±1.22	74.6± 3.6 ±4.9	71
5	0.50±0.05	1.31±0.38	2.54±0.73	0.53±0.38	13.8± 0.9 ±0.9	12
6	0.08±0.02	0.10±0.07	1.09±0.54	0.0±0.0	7.89±0.59±0.51	7
7	0.08±0.02	0.10±0.07	1.09±0.54	0.0±0.0	7.69±0.59±0.50	7
8	0.0±0.0	0.0±0.0	0.87±0.50	0.0±0.0	6.83±0.54±0.44	5

Table 18: Number of background events expected, and number of events observed, after successive selections for an integrated luminosity of $\int \mathcal{L}dt = 318$ pb^{-1} in the $e^{\pm}\mu^{\mp}$ channel for the m_H=160 GeV selection. The statistical error is listed for all backgrounds. The systematical error described in Section 8 without the uncertainty of the integrated luminosity is only given for the sum of all backgrounds.

	$t\bar{t}$	ZZ	WZ	WW
1	15.9±0.2	0.61±0.12	2.69±0.22	42.7±0.5
2	14.4±0.2	0.31±0.09	2.03±0.19	32.7±0.5
3	2.59±0.10	0.13±0.06	1.44±0.16	27.1±0.4
4	1.43±0.07	0.07±0.04	0.67±0.11	17.9±0.4
5	0.93±0.06	0.03±0.03	0.34±0.08	7.33±0.22
6	0.75±0.05	0.03±0.03	0.28±0.07	5.13±0.19
7	0.40±0.04	0.03±0.03	0.28±0.07	5.11±0.19
8	0.37±0.04	0.0±0.0	0.23±0.06	4.69±0.18

	$Z/\gamma^* \to \mu\mu$	$Z/\gamma^* \to \tau\tau$	$W + jet/\gamma$	QCD	Sum	Data
1	26.5±0.6	409±10	66.3±3.8	124±6	688± 13 ±45	691
2	7.31±0.28	65.6±4.0	49.0±3.2	23.1±2.5	195± 6 ±13	174
3	4.75±0.24	26.1±2.4	25.8±2.4	9.84±1.62	97.8± 3.8 ±6.4	90
4	4.18±0.24	25.5±2.4	22.9±2.2	5.85±1.25	78.5± 3.6 ±5.1	75
5	0.65±0.07	0.97±0.32	1.71±0.65	0.27±0.27	12.2± 0.8 ±0.8	13
6	0.21±0.06	0.10±0.07	0.70±0.49	0.0±0.0	7.20±0.54±0.47	7
7	0.21±0.06	0.10±0.07	0.70±0.49	0.0±0.0	6.82±0.54±0.44	7
8	0.0±0.0	0.0±0.0	0.70±0.49	0.0±0.0	5.98±0.53±0.39	5

Table 19: Number of background events expected, and number of events observed, after successive selections for an integrated luminosity of $\int \mathcal{L}\mathrm{d}t = 318$ pb^{-1} in the $e^{\pm}\mu^{\mp}$ channel for the m_H=180 GeV selection. The statistical error is listed for all backgrounds. The systematical error described in Section 8 without the uncertainty of the integrated luminosity is only given for the sum of all backgrounds.

	$t\bar{t}$	ZZ	WZ	WW
1	15.9±0.2	0.61±0.12	2.69±0.22	42.7±0.5
2	14.4±0.2	0.31±0.09	2.03±0.19	32.7±0.5
3	2.59±0.10	0.13±0.06	1.44±0.16	27.1±0.4
4	1.62±0.08	0.07±0.04	0.80±0.12	19.4±0.4
5	1.20±0.07	0.03±0.03	0.40±0.08	6.46±0.21
6	0.93±0.06	0.0±0.0	0.29±0.07	4.32±0.17
7	0.46±0.04	0.0±0.0	0.29±0.07	4.30±0.17
8	0.39±0.04	0.0±0.0	0.25±0.07	3.85±0.16

	$Z/\gamma^* \to \mu\mu$	$Z/\gamma^* \to \tau\tau$	$W + jet/\gamma$	QCD	Sum	Data
1	26.5±0.6	409±10.39	66.3±3.8	124±6.39	688± 13 ±45	691
2	7.31±0.28	65.6±4.0	49.0±3.2	23.1±2.76	195± 6 ±13	174
3	4.75±0.24	26.1±2.4	25.8±2.4	9.84±1.80	97.8± 3.8 ±6.4	90
4	4.50±0.24	25.6±2.4	23.7±2.3	6.21±1.29	81.9±3.67±5.3	79
5	0.73±0.09	0.67±0.24	1.37±0.68	0.27±0.27	11.1± 0.8 ±0.7	12
6	0.21±0.06	0.05±0.05	0.70±0.49	0.27±0.27	6.76±0.61±0.44	6
7	0.21±0.06	0.05±0.05	0.70±0.49	0.27±0.27	6.27±0.61±0.41	6
8	0.0±0.0	0.0±0.0	0.70±0.49	0.0±0.0	5.18±0.52±0.34	3

Table 20: Number of background events expected, and number of events observed, after successive selections for an integrated luminosity of $\int \mathcal{L}dt = 318$ pb^{-1} in the $e^{\pm}\mu^{\mp}$ channel for the m_H=200 GeV selection. The statistical error is listed for all backgrounds. The systematical error described in Section 8 without the uncertainty of the integrated luminosity is only given for the sum of all backgrounds.

m_H	100	120	140	160	180	200
			Signal Efficiencies (%)			
1	3.47±0.08	5.96±0.10	8.10±0.13	8.99±0.14	9.90±0.14	10.61±0.13
2	2.63±0.07	5.04±0.09	7.14±0.13	8.24±0.13	9.18±0.13	9.74±0.13
3	1.84±0.06	3.69±0.08	5.34±0.11	6.36±0.12	7.11±0.12	7.30±0.11
4	1.71±0.06	3.51±0.08	5.03±0.11	6.19±0.11	6.66±0.11	6.41±0.10
5	1.22±0.05	2.47±0.06	3.49±0.09	4.50±0.10	4.68±0.10	4.24±0.08
6	1.06±0.05	2.13±0.06	3.00±0.08	3.99±0.09	4.00±0.09	3.37±0.07
7	1.06±0.05	2.12±0.06	2.99±0.08	3.97±0.09	3.96±0.09	3.31±0.07
8	1.02±0.04	2.04±0.06	2.88±0.08	3.92±0.09	3.91±0.09	3.19±0.07
Exp. Events	0.004±0.001	0.064±0.002	0.211±0.006	0.355±0.008	0.250±0.007	0.114±0.003

Table 21: Efficiencies in % with respect to $H \to WW^{(*)} \to \ell^+\nu\ell'^-\bar{\nu}$ $(\ell, \ell' = e, \mu, \tau_{lep})$ decays for the Higgs signal for six different Higgs masses between 100 and 200 GeV for the different stages of the selection and number of events expected for a standard model Higgs boson at the end of the selection for the $e^\pm\mu^\mp$ final state. Only statistical uncertainties are given.

7.4 The $\mu^+\mu^-$ final state

The event selection for the di–muon channel is as follows: events have been triggered by one of the five triggers as described in Section 4.3. These triggers are required to be not prescaled and to have a good luminosity block number. Runs which are marked bad for muons, $\not\!\!E_T$, SMT, CFT, and calorimeter in the run quality database and certain runs with bad di–muon trigger are rejected. The overall integrated luminosity of this sample is $\mathcal{L} = 299$ pb^{-1}.

Events are required to have two muons of loose quality satisfying the ID criteria described in Section 3.2. The transverse momentum of the leading muon should be $p_T^{\mu_1} > 15$ GeV, whereas the trailing muon should have $p_T^{\mu_2} > 10$ GeV.

Figure 21 shows the distributions of the invariant di–muon mass $m_{\mu\mu}$ and the missing transverse energy $\not\!\!E_T$ after application of all cuts described above, with an additional lower cut boundary of $m_{\mu\mu} > 20\,\text{GeV}$. Similarly Figure 22 shows distributions of the muon transverse momenta p_T and and the muon azimuthal opening angle $\Delta\phi_{\mu\mu}$. The discrepancy between data and Monte Carlo for high transverse momentum and high invariant di–muon masses $m_{\mu\mu}$ can be explained with decreasing momentum resolution for tracks with increasing transverse momentum which is not modeled by a simple Gaussian smearing of the Monte Carlo as explained in Section 5.

To suppress backgrounds with similar event topologies as $H \to WW^{(*)}$ production a set of cuts is applied as described in Section 7.1. This selection is applied for Higgs masses m_H= 100, 120, 180, 200 GeV.

For Higgs masses m_H= 140 and 160 GeV a slightly changed selection is applied to give the best exclusion limit in Section 9. Cuts 4, 5 and 6 are exchanged by the following cuts: The invariant mass $m_{\mu\mu}$ should be in the range $20\,\text{GeV} < m_{\mu\mu} < 80\,\text{GeV}$ (Cut 4). Since the momentum resolution is decreasing for tracks with high transverse momentum an additional constrained fit of all events is performed testing if these events are compatible with Z boson production. This fit uses a χ^2 minimization with a Z mass constraint and $p_T^{\mu_1}$ as the variation parameter for MINUIT:

$$\begin{aligned}\chi^2_\text{fit} = & \left(\frac{1/p_T^{\mu_1} - 1/p_T^{\mu_1,fit}}{1/\Delta p_T^{\mu_1}}\right)^2 \\ & + \left(\frac{1/p_T^{\mu_2} - 1/p_T^{\mu_2,fit}}{1/\Delta p_T^{\mu_2}}\right)^2 \\ & + \left(\frac{\vec{p}_T^{\,Had} + \vec{p}_T^{\,\mu_1,fit} + \vec{p}_T^{\,\mu_2,fit}}{\Delta p_T^{Had+\mu_1+\mu_2}}\right)^2\end{aligned} \tag{14}$$

The hadronic recoil of the Z defined as all jets in the event is calculated from the sum of the missing transverse momentum $\not\!\!E_T$ and the muon momenta in the event. All errors are derived from a parameterization of the MC corresponding to the data resolution.

The best signal efficiency over background rejection is achieved by a cut on $\chi^2_{\mathrm{fit}} > 20$ (Cut 5). The sum of the muon transverse momenta and the missing transverse energy should be $p_{\mathrm{T}}^{\mu 1} + p_{\mathrm{T}}^{\mu 2} + \not\!\!E_T > 90\,\mathrm{GeV}$ (Cut 6). Table 22 summarizes the 3 different cuts that are used instead compared to the mass dependent selection.

Figure 24 shows the distribution of the χ^2_{fit} of the constrained fit before cut 1 (top left), the scalar sum H_T after cut 6 (top right), the invariant di–muon mass $m_{\mu\mu}$ before the last cut (bottom left) and the muon azimuthal opening angle $\Delta\phi_{\mu\mu}$ after all cuts (bottom right).

The expectations from all the backgrounds after all cuts is between 6.8±0.7 (stat) ± 0.5 (syst) and 13.1±1.1 (stat) ±2.3 (syst) events depending on the selection. The $Z/\gamma^* \to \mu\mu$ decays always contribute more than half to this background expectation. Because of the worse momentum resolution of the muons compared to the electrons this background has a larger contribution after the final selection in contrary to the di–electron channel. Tables 23, 24, 25, 26 and 27 summarize the expected numbers for all backgrounds compared with the data for all different selection criteria.

The efficiency for $H \to WW^{(*)} \to \ell^+\nu\ell'^-\bar{\nu}$ $(\ell, \ell' = e, \mu, \tau_{lep})$ production at the beginning of the selection is (4.6±0.9)% for $m_H = 200$ GeV. Applying all different selection criteria reduces the efficiency to (0.44±0.03)% to (2.00±0.06)% depending on the selection. Table 28 summarizes efficiencies and the number of expected events from $H \to WW^{(*)}$ decays after all cuts dependent on the Higgs boson mass m_H. Using these efficiencies and the cross sections from Table 3, 0.145 ± 0.005 Higgs events are expected for a Higgs mass of $m_H = 160$ GeV and 0.026 ± 0.001 Higgs events for a Higgs mass of $m_H = 120$ GeV.

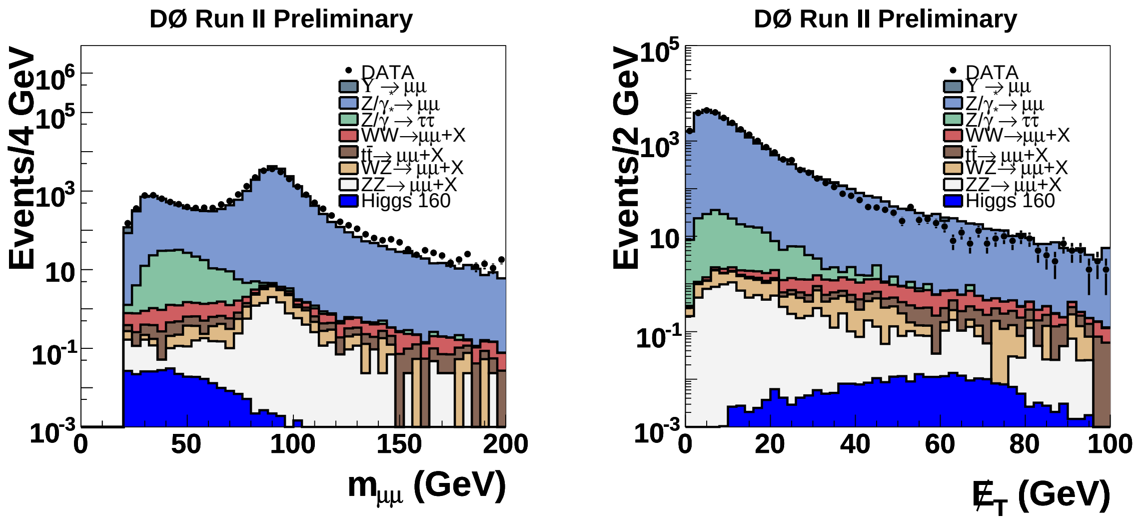

Figure 21: Distribution of the invariant di–muon mass $m_{\mu\mu}$ (left) and the missing transverse energy $\not\!\!E_T$ (right) after the preselection for the $\mu^+\mu^-$ channel.

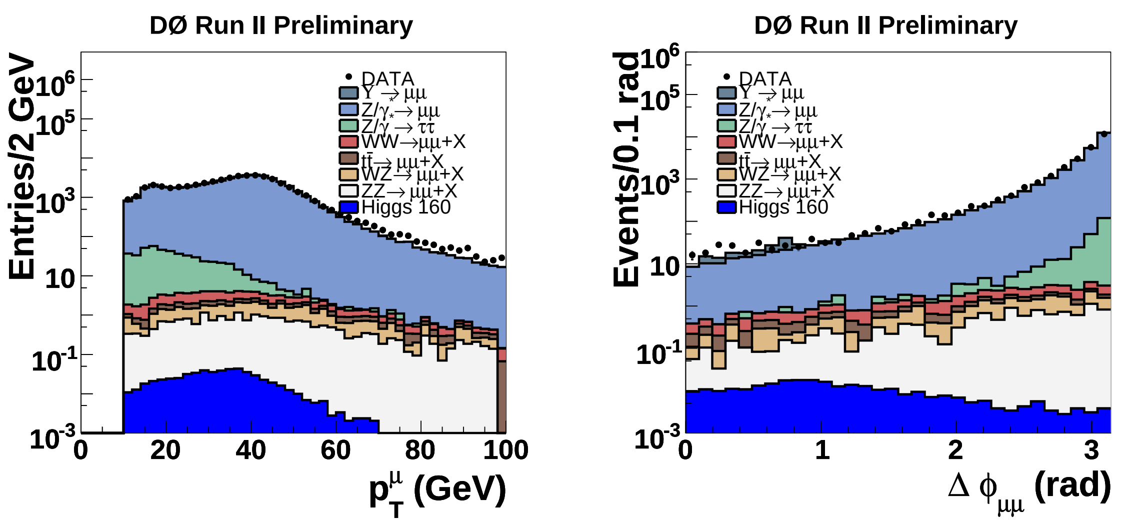

Figure 22: Distribution of the muon transverse momenta p_{T} (left) and the muon azimuthal opening angle $\Delta\phi_{\mu\mu}$ (right) after the preselection for the $\mu^+\mu^-$ channel.

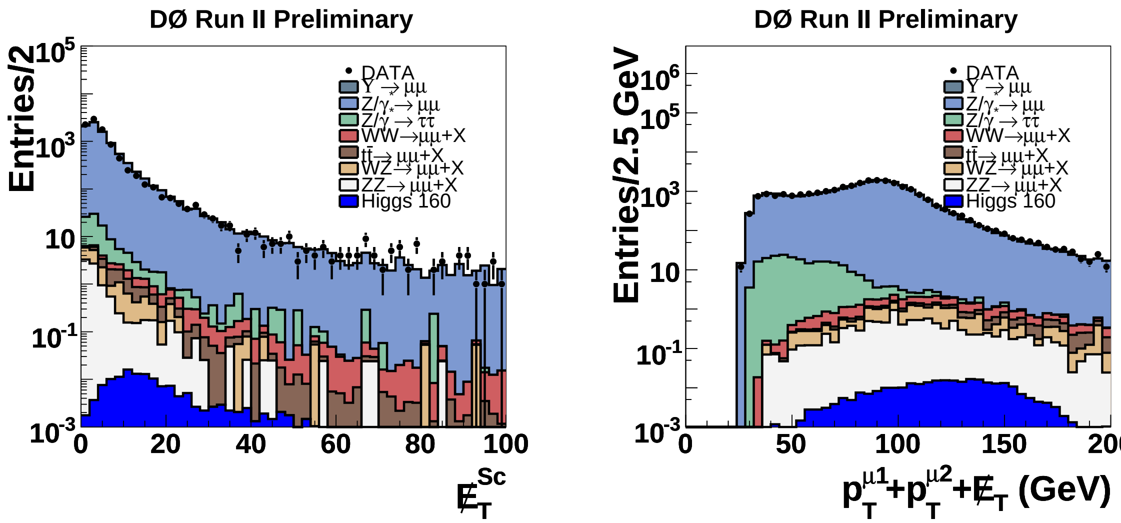

Figure 23: Distribution of the scaled missing transverse energy $\not{E}_T^{\rm Sc}$ (left) and the sum of the muon transverse momenta and missing transverse energy (right) after the preselection for the $\mu^+\mu^-$ channel.

	Selection criterion	Value
Cut 1	Preselection	Trigger, ID, leptons with opposite charge and $p_T^{\ell_1} > 15$ GeV and $p_T^{\ell_2} > 10$ GeV
Cut 2	Missing transverse energy $\not{E}_T$	$\not{E}_T > 20\,$GeV
Cut 3	Scaled $\not{E}_T^{\rm Sc}$	$\not{E}_T^{\rm Sc} > 15$ (for $N_{Jet} > 0$)
Cut 4	Invariant mass $m_{\mu\mu}$	$20\,\mathrm{GeV} < m_{\mu\mu} < 80\,\mathrm{GeV}$
Cut 5	constraint Z fit	$\chi^2 > 20.$
Cut 6	Sum of $p_{\rm T}$ and $\not{E}_T$	$p_{\rm T}^{\mu1} + p_{\rm T}^{\mu2} + \not{E}_T > 90\,$GeV
Cut 7	H_T (scalar sum of p_T^{Jet})	$H_T^{Jet} < 100\,$GeV
Cut 8	Lepton opening angle $\Delta\phi_{\ell\ell}$	$\Delta\phi_{\ell\ell} < 2.0$

Table 22: Summary of the additional selection criteria for m_H= 140 and 160 GeV the $\mu^+\mu^-$ final state.

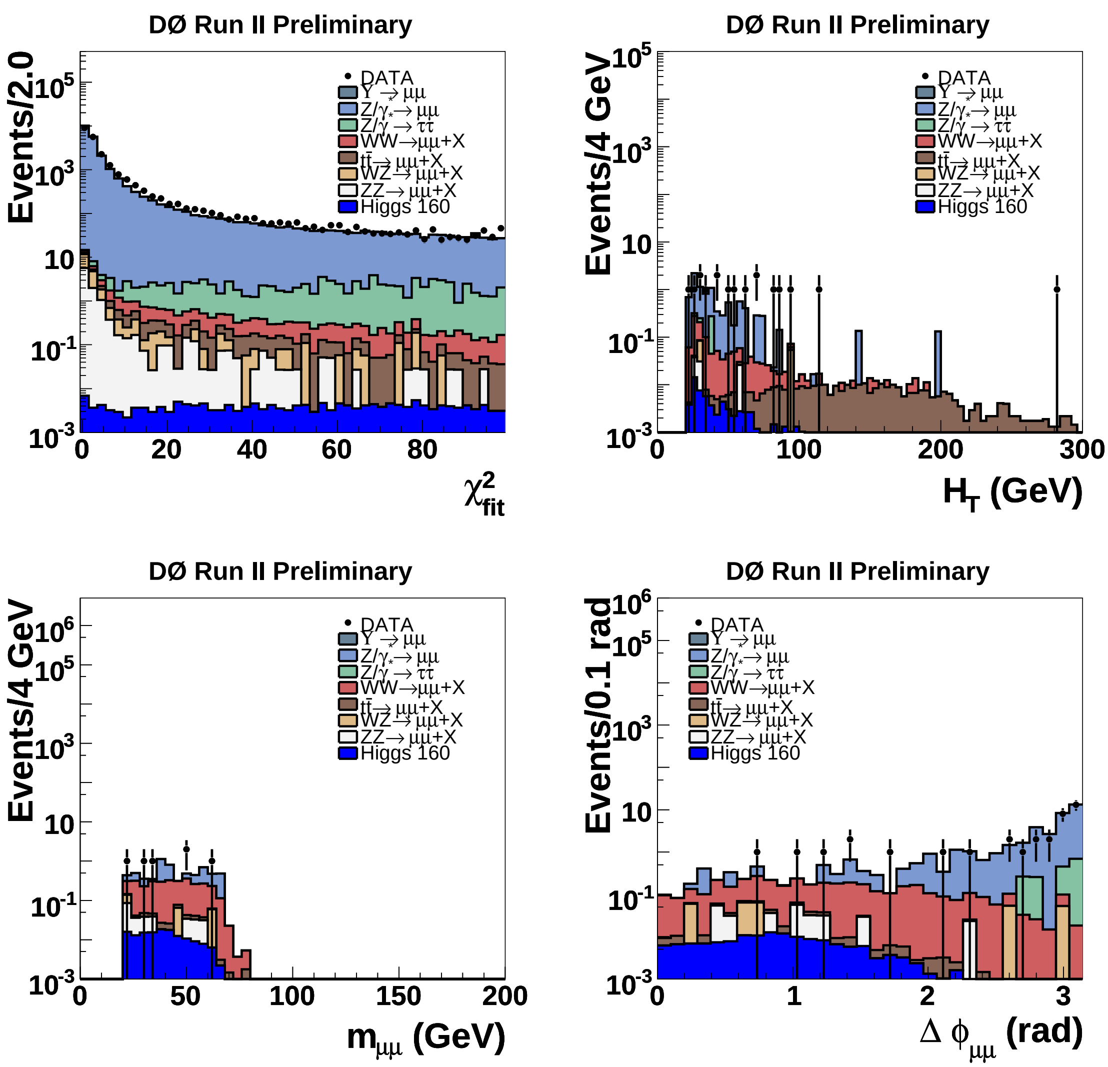

Figure 24: Distribution of χ^2_{fit} of the constrained fit after cut 1 (top left) scalar sum H_T of the transverse energy of all good jets after cut 5, where only events with at least one good jet are shown (top right), the invariant di–muon mass $m_{\mu\mu}$ after all cuts (bottom left) and the muon opening angle $\Delta\phi_{\mu\mu}$ in the transverse plane before the last cut (bottom right). All distributions are shown for the $\mu^+\mu^-$ final state.

	$t\bar{t}$	WZ	ZZ	WW	Υ
1	7.1±0.1	12.5±0.8	11.4±0.5	18.1±0.3	94.8±22.7
2	6.5±0.1	6.1±0.6	4.2±0.3	15.0±0.2	16.7±8.7
3	1.37±0.02	3.3±0.4	2.1±0.2	11.9±0.2	0.0±0.0
4	0.29±0.01	0.16±0.1	0.1±0.1	3.3±0.1	0.0±0.0
5	0.022±0.003	0.05±0.08	0.0±0.0	1.50±0.07	0.0±0.0
6	0.017±0.003	0.00±0.00	0.0±0.0	1.20±0.07	0.0±0.0
7	0.004±0.001	0.00±0.00	0.0±0.0	1.19±0.07	0.0±0.0
8	0.004±0.001	0.00±0.00	0.0±0.0	0.98±0.06	0.0±0.0

	$Z/\gamma^* \to \tau\tau$	$Z/\gamma^* \to \mu\mu$	$W + jet$ QCD	Sum	Data
1	226.8±7.2	26325.8±59.2	42.0±4.0	26738.7±63.2±1873.6	27070
2	35.0±2.7	3120.7±20.4	17.1±1.8	3221.4±21.3±356.7	2984
3	19.2±2.0	1154.3±12.8	1.6±0.3	1194.0±13.0±187.6	1395
4	9.3±1.3	34.1±2.1	0.9±0.2	48.3± 2.5 ±3.2	67
5	8.8±1.3	26.2±1.9	0.6±0.1	37.2± 2.3 ±2.5	42
6	2.9±0.8	18.6±1.6	0.4±0.1	23.1± 1.8 ±1.6	17
7	2.9±0.8	18.4±1.6	0.4±0.1	23.0± 1.8 ±1.6	16
8	0.0±0.0	6.7±1.0	0.3±0.1	8.0± 1.0 ±0.6	4

Table 23: Number of background events expected, and number of events observed, after successive selections for an integrated luminosity of $\int \mathcal{L}dt = 299$ pb^{-1} in the $\mu^+\mu^-$ channel for the m_H=100 GeV selection. The statistical error is listed for all backgrounds. The systematical error described in Section 8 without the uncertainty of the integrated luminosity is only given for the sum of all backgrounds.

	$t\bar{t}$	WZ	ZZ	WW	Υ
1	7.1±0.1	12.5±0.8	11.4±0.5	18.1±0.3	94.8±22.7
2	6.5±0.1	6.1±0.6	4.2±0.3	15.0±0.2	16.7±8.7
3	1.37±0.02	3.3±0.4	2.1±0.2	11.9±0.2	0.0±0.0
4	0.42±0.01	0.2±0.1	0.2±0.1	4.6±0.1	0.0±0.0
5	0.072±0.005	0.05±0.05	0.09±0.05	2.8±0.1	0.0±0.0
6	0.057±0.005	0.00±0.00	0.07±0.05	2.0±0.09	0.0±0.0
7	0.024±0.003	0.00±0.00	0.07±0.05	2.0±0.09	0.0±0.0
8	0.019±0.003	0.00±0.00	0.02±0.02	1.7±0.08	0.0±0.0

	$Z/\gamma^* \to \tau\tau$	$Z/\gamma^* \to \mu\mu$	$W + jet$ QCD	Sum	Data
1	226.8±7.2	26325.8±59.2	42.0±4.0	26738.7±63.2±1873.6	27070
2	35.0±2.7	3120.7±20.4	17.1±1.8	3221.4±21.3±356.7	2984
3	19.2±2.0	1154.3±12.8	1.6±0.3	1194.0±13.0±187.6	1395
4	15.3±1.8	77.5±3.2	0.8±0.2	140.3± 3.7 ±6.9	107
5	11.1±1.6	61.8±2.8	0.6±0.1	93.0± 3.2 ±5.2	59
6	2.1±0.6	26.5±1.8	0.4±0.1	32.3± 1.9 ±2.0	17
7	2.1±0.6	26.4±1.8	0.4±0.1	31.4± 1.9 ±2.0	16
8	0.0±0.0	6.8±1.0	0.3±0.1	8.8± 1.0 ±0.6	7

Table 24: Number of background events expected, and number of events observed, after successive selections for an integrated luminosity of $\int \mathcal{L}dt = 299$ pb^{-1} in the $\mu^+\mu^-$ channel for the m_H=120 GeV selection. The statistical error is listed for all backgrounds. The systematical error described in Section 8 without the uncertainty of the integrated luminosity is only given for the sum of all backgrounds.

	$t\bar{t}$	WZ	ZZ	WW	Υ
1	7.1±0.1	12.5±0.8	11.4±0.5	18.1±0.3	94.8±22.7
2	6.5±0.1	6.1±0.6	4.2±0.3	15.0±0.2	16.7±8.7
3	1.37±0.02	3.3±0.4	2.1±0.2	11.9±0.2	0.0±0.0
4	0.63±0.02	0.8±0.2	0.4±0.1	7.0±0.2	0.0±0.0
5	0.39±0.01	0.3±0.1	0.19±0.07	5.3±0.1	0.0±0.0
6	0.37±0.01	0.2±0.1	0.16±0.07	3.5±0.1	0.0±0.0
7	0.010±0.006	0.2±0.1	0.16±0.07	3.5±0.1	0.0±0.0
8	0.088±0.006	0.16±0.09	0.12±0.06	2.8±0.1	0.0±0.0

	$Z/\gamma^* \to \tau\tau$	$Z/\gamma^* \to \mu\mu$	$W + jet$ QCD	Sum	Data
1	226.8±7.2	26325.8±59.2	42.0±4.0	26738.7±63.2±1873.6	27070
2	35.0±2.7	3120.7±20.4	17.1±1.8	3221.4±21.2±356.7	2984
3	19.2±2.0	1154.3±12.8	1.6±0.3	1194.0±13.0±187.6	1395
4	18.7±1.9	202.4±5.2	0.9±0.2	230.9± 5.6 ±26.2	231
5	17.3±1.9	104.6±3.7	0.7±0.1	129.0± 4.2 ±9.4	124
6	2.3±0.6	39.1±2.1	0.4±0.1	46.2± 2.2 ±2.9	38
7	2.3±0.6	38.5±2.1	0.4±0.1	45.4± 2.2 ±2.8	36
8	0.0±0.0	3.4±0.6	0.2±0.1	6.8± 0.7 ±0.5	6

Table 25: Number of background events expected, and number of events observed, after successive selections for an integrated luminosity of $\int \mathcal{L}dt = 299\ \mathrm{pb}^{-1}$ in the $\mu^+\mu^-$ channel for the m_H=140 and 160 GeV selection. The statistical error is listed for all backgrounds. The systematical error described in Section 8 without the uncertainty of the integrated luminosity is only given for the sum of all backgrounds.

	$t\bar{t}$	WZ	ZZ	WW	Υ
1	7.1±0.1	12.5±0.8	11.4±0.5	18.1±0.3	94.8±22.7
2	6.5±0.1	6.1±0.6	4.2±0.3	15.0±0.2	16.7±8.7
3	1.37±0.02	3.3±0.4	2.1±0.2	11.9±0.2	0.0±0.0
4	0.74±0.02	2.4±0.3	1.0±0.1	7.8±0.2	0.0±0.0
5	0.445±0.014	1.5±0.2	0.7±0.1	4.7±0.1	0.0±0.0
6	0.376±0.013	0.8±0.1	0.40±0.09	3.3±0.1	0.0±0.0
7	0.102±0.007	0.8±0.1	0.40±0.09	3.3±0.1	0.0±0.0
8	0.091±0.006	0.42±0.09	0.26±0.08	2.9±0.1	0.0±0.0

	$Z/\gamma^* \to \tau\tau$	$Z/\gamma^* \to \mu\mu$	$W + jet$ QCD	Sum	Data
1	226.8±7.2	26325.8±59.2	42.0±4.0	26738.7±63.2±1873.6	27070
2	35.0±2.7	3120.7±20.4	17.1±1.8	3221.4±21.3±356.7	2984
3	19.2±2.0	1154.3±12.8	1.6±0.3	1194.0±13.0±187.6	1395
4	18.9±2.0	403.8±7.7	1.0±0.2	434.9± 8.0 ±73.5	371
5	1.2±0.5	219.5±5.8	0.7±0.1	228.3± 5.8 ±49.8	204
6	0.4±0.3	22.7±1.8	0.4±0.1	28.1± 1.9 ±3.3	16
7	0.4±0.3	18.0±1.6	0.4±0.1	23.1± 1.7 ±4.0	15
8	0.0±0.0	6.2±0.9	0.3±0.1	10.2± 0.9 ±1.4	8

Table 26: Number of background events expected, and number of events observed, after successive selections for an integrated luminosity of $\int \mathcal{L} dt = 299$ pb^{-1} in the $\mu^+\mu^-$ channel for the m_H=180 GeV selection. The statistical error is listed for all backgrounds. The systematical error described in Section 8 without the uncertainty of the integrated luminosity is only given for the sum of all backgrounds.

	$t\bar{t}$	WZ	ZZ	WW	Υ
1	7.1±0.1	12.5±0.8	11.4±0.5	18.1±0.3	94.8±22.7
2	6.5±0.1	6.1±0.6	4.2±0.3	15.0±0.2	16.7±8.7
3	1.37±0.02	3.3±0.4	2.1±0.2	11.9±0.2	0.0±0.0
4	0.82±0.02	0.8±0.3	1.6±0.2	8.5±0.2	0.0±0.0
5	0.56±0.02	0.3±0.3	1.1±0.2	4.4±0.1	0.0±0.0
6	0.46±0.01	0.2±0.2	0.68±0.1	3.0±0.1	0.0±0.0
7	0.115±0.007	0.2±0.2	0.68±0.1	2.9±0.1	0.0±0.0
8	0.101±0.007	0.16±0.1	0.37±0.09	2.5±0.1	0.0±0.0

	$Z/\gamma^* \to \tau\tau$	$Z/\gamma^* \to \mu\mu$	$W + jet$ QCD	Sum	Data
1	226.8±7.2	26325.8±59.2	42.0±4.0	26738.7±63.2±1873.6	27070
2	35.0±2.7	3120.7±20.4	17.1±1.8	3221.4±21.3±356.7	2984
3	19.2±2.0	1154.3±12.8	1.6±0.3	1194.0±13.0±187.6	1395
4	18.9±2.0	682.5±10.0	1.4±0.2	716.2±10.2±117.1	607
5	0.7±0.3	327.3±6.9	0.7±0.1	336.2± 6.9 ±58.0	325
6	0.1±0.3	35.9±2.1	0.5±0.1	41.5± 2.1 ±4.4	21
7	0.1±0.3	25.7±1.8	0.5±0.1	30.8± 1.8 ±5.7	20
8	0.0±0.0	9.7±1.1	0.3±0.1	13.1± 1.1 ±2.3	8

Table 27: Number of background events expected, and number of events observed, after successive selections for an integrated luminosity of $\int \mathcal{L}dt = 299$ pb^{-1} in the $\mu^+\mu^-$ channel for the m_H=200 GeV selection. The statistical error is listed for all backgrounds. The systematical error described in Section 8 without the uncertainty of the integrated luminosity is only given for the sum of all backgrounds.

m_H	100	120	140	160	180	200
			Signal Efficiencies (%)			
1	1.60±0.06	2.76±0.07	3.67±0.09	4.06±0.09	4.14±0.09	4.60±0.09
2	1.24±0.05	2.49±0.06	3.39±0.09	3.84±0.09	3.92±0.09	4.31±0.09
3	0.82±0.04	1.72±0.05	2.37±0.08	2.83±0.08	2.88±0.08	3.16±0.07
4	0.71±0.04	1.59±0.05	2.27±0.07	2.71±0.07	2.64±0.07	2.70±0.07
5	0.57±0.03	1.30±0.05	2.05±0.07	2.49±0.06	2.12±0.06	2.10±0.06
6	0.50±0.03	1.15±0.04	1.58±0.06	2.20±0.06	1.84±0.06	1.79±0.05
7	0.50±0.03	1.13±0.04	1.49±0.06	2.07±0.06	1.75±0.06	1.65±0.05
8	0.44±0.03	1.02±0.04	1.34±0.05	2.00±0.06	1.68±0.06	1.53±0.05
Exp. Events	0.0014±0.0001	0.026±0.001	0.079±0.003	0.145±0.005	0.085±0.003	0.043±0.001

Table 28: Efficiencies in % with respect to $H \to WW^{(*)} \to \ell^+\nu\ell'^-\bar{\nu}$ $(\ell, \ell' = e, \mu, \tau_{lep})$ decays for the Higgs signal for six different Higgs masses between 100 and 200 GeV for the different stages of the selection and number of events expected for a standard model Higgs boson at the end of the selection for the $\mu^+\mu^-$ final state. Only statistical uncertainties are given.

8 Systematic studies

Various sources of systematic uncertainties have been studied to investigate their influence on the expected background events and the signal efficiency of $H \to WW^{(*)}$ production in the various channels.

8.1 The e^+e^- final state

- The jet energy scale was varied by $\pm 1\sigma$.
- The influence of the electron momentum smearing was tested by changing the smearing parameter f and the calibration factor c by $\pm 1\sigma$.
- The Z/γ^* cross section is varied within the theoretical uncertainty of $\pm 3.6\%$.
- The influence of the $t\bar{t}$ cross section is also tested. It is varied by $+5.9\%$ and -14.7%.
- The WW production cross section is varied by $\pm 8.0\%$.
- To test the systematic dependence caused by electron reconstruction efficiencies as well as trigger efficiencies, all these parameters were changed within $\pm 1\sigma$.
- The PDF eigenvectors with the highest variation of the signal process cross section have been identified. The deviation of the signal acceptance by the use of these parameters instead of the default values determines the PDF uncertainty of the signal processes. The PDF uncertainties on the different background processes are included in the variation of the different background cross sections.

In the low mass region, the uncertainty is dominated by the jet energy scale and variations in the $W+jet/\gamma$ contribution. With increasing Higgs mass, this uncertainty is decreasing because of the decreasing contribution of $W+jet/\gamma$ events. Since the WW production is the dominant background for Higgs bosons above $m_H = 160$ GeV, the systematic uncertainty is dominated by the error on the WW production cross section. Table 29 summarizes the systematic uncertainties for background and signal for all six Higgs masses.

8.2 The $e^{\pm}\mu^{\mp}$ final state

- The jet energy scale is varied within $\pm 1\sigma$.
- The influence of the muon resolution was tested by varying the parameters by $\pm 1\sigma$. The same was done for the electron resolution.

m_H [GeV]	100	120	140	160	180	200
	Change of the Background (%)					
JES	+4.3	+3.6	+3.1	+1.3	+2.3	+1.6
	−4.1	−3.2	−3.4	−1.1	−2.8	−4.6
Electron ID, trigger	+2.6	+2.6	+2.6	+2.6	+2.6	+2.6
	−2.6	−2.6	−2.6	−2.6	−2.6	−2.6
Electron resolution	+0.5	+0.5	+0.6	+0.4	+0.3	+1.6
	−0.7	−0.4	−0.7	−0.2	−0.3	−0.8
WW cross section	+1.0	+1.2	+2.7	+4.6	+6.4	+6.0
	−1.0	−1.3	−2.8	−4.8	−6.8	−6.4
$t\bar{t}$ cross section	–	–	–	+0.1	+0.3	+0.8
	–	–	–	−0.3	−1.0	−1.7
Z/γ^* cross section	+0.4	+0.5	+0.4	+0.4	+0.2	–
	−0.4	−0.5	−0.4	−0.4	−0.2	–
Total BG error (%)	+5.2	+4.7	+4.9	+5.5	+7.3	+7.0
	−4.9	−4.4	−5.2	−5.6	−7.9	−8.5
Signal Efficiency error (%)	8.3	8.3	6.4	6.6	6.9	6.8

Table 29: Summary of the systematic uncertainties on the number of background events excluding the uncertainty on the luminosity measurement and the uncertainty on the $H \to WW^{(*)}$ signal efficiency for the e^+e^- channel.

- The cross sections for Z/γ^*, WW, and $t\bar{t}$ production were varied within $\pm 1\sigma$ of the theoretical uncertainty.
- To test the systematic dependence caused by electron and muon reconstruction efficiencies as well as trigger efficiencies, all these parameters were changed within $\pm 1\sigma$.
- The PDF uncertainty was determined as described in Section 8.1.

For low mass Higgs bosons the systematic uncertainty is dominated by the uncertainty of the jet energy scale. In addition, the uncertainty of the WW production cross section is also of importance. With increasing Higgs mass, this uncertainty becomes the dominant factor, since the WW production is the most important background contribution. The influence from the jet energy scale uncertainty decreases. The systematic uncertainties from the electron and muon resolutions are negligible. Table

30 summarizes the total systematic uncertainty for background and signal for all six Higgs masses.

m_H [GeV]	100	120	140	160	180	200
	Change of the Background (%)					
JES	+4.4	+9.4	+8.3	+4.1	+3.5	+4.7
	−3.4	−5.7	−3.7	−2.4	−2.2	−2.7
Electron ID, Trigger	+2.0	+2.0	+2.0	+2.0	+2.0	+2.0
	−2.0	−2.0	−2.0	−2.0	−2.0	−2.0
Muon ID, Trigger	+2.7	+2.7	+2.7	+2.7	+2.7	+2.7
	−2.7	−2.7	−2.7	−2.7	−2.7	−2.7
Electron resolution	+0.5	+0.4	+0.3	+0.8	+0.5	+0.8
	−0.5	−0.4	−0.3	−0.9	−0.5	−0.7
Muon resolution	+1.2	+0.3	+0.2	+0.5	+0.8	+0.5
	−1.6	−1.6	−0.2	−0.4	−0.8	−0.3
WW cross section	+1.5	+2.9	+4.6	+5.7	+6.4	+6.4
	−1.6	−3.0	−4.8	−6.1	−6.8	−6.8
$t\bar{t}$ cross section	–	–	+0.1	+0.2	+0.2	+0.5
	–	−0.1	−0.2	−0.4	−1.0	−1.4
Z/γ^* cross section	+0.1	+0.1	–	–	–	–
	−0.1	−0.1	–	–	–	–
Total BG error (%)	+5.9	+10.4	+10.1	+7.9	+8.1	+8.7
	−5.3	−7.5	−6.9	−7.4	−8.0	−8.2
Signal Efficiency error (%)	6.4	6.7	6.9	6.7	6.6	6.1

Table 30: Summary of the systematic uncertainties on the number of background events excluding the uncertainty on the luminosity measurement and the uncertainty on the $H \rightarrow WW^{(*)}$ signal efficiency for the $e^{\pm}\mu^{\mp}$ channel.

8.3 The $\mu^+\mu^-$ final state

- The change of the jet energy scale correction was tested by altering the correction by $\pm 1\sigma$. The change of the number of background events ranges from 2.5% for a m_H= 100 GeV selection to $\approx$ 12% for a m_H= 200 GeV selection.
- The muon momentum smearing was varied by $\pm 1\sigma$ of the parameter f. The change of the number of background events ranges from $\pm$1% for a m_H= 100 GeV selection to $\pm$6.4% for a m_H= 160 GeV selection.

- The cross sections of $Z/\gamma^* \to \mu\mu$, WW and $t\bar{t}$ production were lowered and raised simultaneously within their theoretical error of $\pm 3.6\%$ for $Z/\gamma^* \to \mu\mu$, $\pm 8\%$ for WW and $+5.9\%$ or -14.7% for $t\bar{t}$ production. The number of background events changes by about $\pm 3.0\%$ for all different selections.

- The trigger efficiency and efficiency for muon reconstruction was altered by $\pm 1\sigma$. The number of background events changes by about $\pm 3.1\%$ for all different selections.

- The PDF uncertainty was determined as described in Section 8.1.

The variation of the jet energy scale is the main uncertainty for the selection of high Higgs masses with about 11%. The uncertainty on the selection efficiency for $H \to WW^{(*)}$ decays is in the same range of the statistical uncertainty error. Table 31 summarizes the systematic uncertainties for the different selections.

m_H [GeV]	100	120	140	160	180	200
	Change of the Background (%)					
JES	± 0.0	± 0.0	$+1.1$	$+1.1$	$+9.4$	$+10.9$
	-2.5	-1.2	-0.4	-0.4	-9.4	-12.2
Muon resolution	$+1.0$	$+3.7$	± 0.0	± 0.0	± 0.0	$+4.5$
	-1.3	-1.5	-6.4	-6.4	-1.3	± 0.0
Z/γ^*, WW, $t\bar{t}$ cross section	$+3.5$	$+3.2$	$+1.9$	$+1.9$	$+2.7$	$+2.9$
	-3.5	-3.2	-2.0	-2.0	-2.8	-3.0
Muon ID, Trigger	$+3.1$	$+3.1$	$+3.1$	$+3.1$	$+3.1$	$+3.1$
	-3.1	-3.1	-3.1	-3.1	-3.1	-3.1
Total BG error	$+4.8$	$+5.8$	$+3.7$	$+3.7$	$+10.3$	$+13.7$
	-5.4	-4.8	-7.5	-7.5	-10.4	-11.8
Signal Efficiency error (%)	7.8	7.3	7.2	7.1	7.3	6.9

Table 31: Summary of the systematic uncertainties on the number of background events excluding the uncertainty on the luminosity measurement and the uncertainty on the $H \to WW^{(*)}$ signal efficiency for the $\mu^+\mu^-$ channel.

9 Limits

Since after all selection cuts the remaining candidate events are consistent with a background observation, limits on the production cross section times branching ratio $\sigma \times BR(H \rightarrow WW^{(*)})$ are derived following the modified frequentist method described in Ref. [37]. It provides the confidence level for the background to represent the data, CL_B, and the confidence level for the sum of signal and background hypothesis CL_{S+B} with the possible use of the expected opening angle distribution $\Delta\phi_{\ell\ell}$ for signal and background. The 95% CL limit for signal is defined as $CL_S = CL_{S+B}/CL_B$, requiring $CL_S = 0.05$. The systematic errors on the background expectation and signal efficiencies as described in section 8 are used. In addition a systematic uncertainty of 6.5% on the luminosity measurement is used.

Table 32 and Table 33 sum up the individual observed and expected upper limits on the cross section times branching ratio for the three different decay channels for six different Higgs boson masses m_H. The calculation of the individual limits was done as described above using only the number expected background and signal events with their corresponding uncertainties and the number of observed events (1 bin). This method provides very similar results like the bayesian limit setting procedure described in Ref. [38]. The different values of the upper limits for the three different channels especially for the two lowest mass points are a consequence of the different background contributions and lower signal efficiencies.

Both tables also show the results of the observed and expected limits for the combination of all three channels. Two methods have been used: as for the individual channels the first combination result uses only the number of expected background and signal events with their corresponding uncertainties and the number of observed events per channel (1 bin). The individual values of CL_B are shown as well. A value of $CL_B = 0.5$ indicates the background to represent the data reasonably well. The denoted second results use the expected opening angle distribution $\Delta\phi_{\ell\ell}$ in 32 bins for signal, background and data and their corresponding uncertainties per channel before the final cut on this variable (see e.g. Figure 24 bottom right). This method provides the possibility to further discriminate between signal and background in distributions where both reasonably differ. The expected limits improve by about 20-30% while the observed limits are almost unchanged.

Figure 25 shows the results of the expected and observed limits for the combination in 1 bin per channel together with expectations from standard model Higgs boson production and alternative models for the current amount of luminosity. While much more data is needed to get sensitivity for a standard model Higgs boson, alternative models with additional generations of quarks [40] are already accessible with the current data set. Models assuming six generations of quarks and one neutrino with $m_N = 50$ GeV ($\mathrm{SM}-6^*$) can be ruled out for Higgs masses between 160 and 200 GeV, while the current analysis falls short of excluding models with only two additional generations

(SM − 5*). A factor of 2–3 in sensitivity is needed to exclude models with four quark generations (SM − 4, SM − 4*).

A projection to future integrated luminosities has been done. The luminosity and its error, the number of expected background and data events are scaled by a factor of x. The expected background errors are scaled by a factor of $\sqrt{x}$. Figure 26 shows the projected exclusion limits for 2 and 16 fb^{-1} assuming the efficiencies and errors of the current analysis. The luminosity of $16 = 2 \times 8$ fb^{-1} corresponds to the expected combination of the full Run II dataset to be taken by the DØ and CDF experiment. With the current signal efficiencies and errors on the background expectation and luminosity it is not possible to exclude parts of the standard model Higgs boson mass range with the full Run II dataset. Improved efficiencies of the lepton identification and better background suppression methods can provide better exclusion limits in the future.

m_H [GeV]	100	120	140	160	180	200
observed limit $\sigma \times BR(H \to WW^{(*)})$ [pb]						
e^+e^-	51.9	18.9	20.5	12.8	12.9	10.8
$e^\pm\mu^\mp$	31.3	8.1	5.3	4.7	4.9	4.7
$\mu^+\mu^-$	37.1	21.4	16.2	10.9	13.9	14.4
combination (1 bin)	18.5	5.6	4.9	3.7	4.1	3.2
CL_B	0.41	0.06	0.30	0.41	0.59	0.16
combination (32 bin)	19.2	7.64	5.0	3.7	3.9	3.1
CL_B	0.43	0.61	0.63	0.73	0.73	0.34

Table 32: Observed upper limits at 95% C.L. on the cross section times branching ratio for $\sigma \times BR(H \to WW^{(*)})$ from the e^+e^-, $e^\pm\mu^\mp$, $\mu^+\mu^-$ final state and the combination in 1 bin and 32 bins of the $\Delta\phi_{\ell\ell}$ distribution of all three channels for different Higgs boson masses m_H.

m_H [GeV]	100	120	140	160	180	200
expected limit $\sigma \times BR(H \to WW^{(*)})$ [pb]						
e^+e^-	51.9	25.2	14.5	9.7	7.8	10.8
$e^\pm\mu^\mp$	28.6	12.4	7.7	6.0	5.6	6.3
$\mu^+\mu^-$	59.8	26.9	18.5	12.3	17.2	22.1
combination (1 bin)	20.3	9.5	5.9	4.0	3.9	4.5
combination (32 bin)	20.1	6.8	4.4	3.1	3.1	3.6

Table 33: Expected upper limits at 95% C.L. on the cross section times branching ratio for $\sigma \times BR(H \to WW^{(*)})$ from the e^+e^-, $e^\pm\mu^\mp$, $\mu^+\mu^-$ final state and the combination in 1 bin and 32 bins of the $\Delta\phi_{\ell\ell}$ distribution of all three channels for different Higgs boson masses m_H.

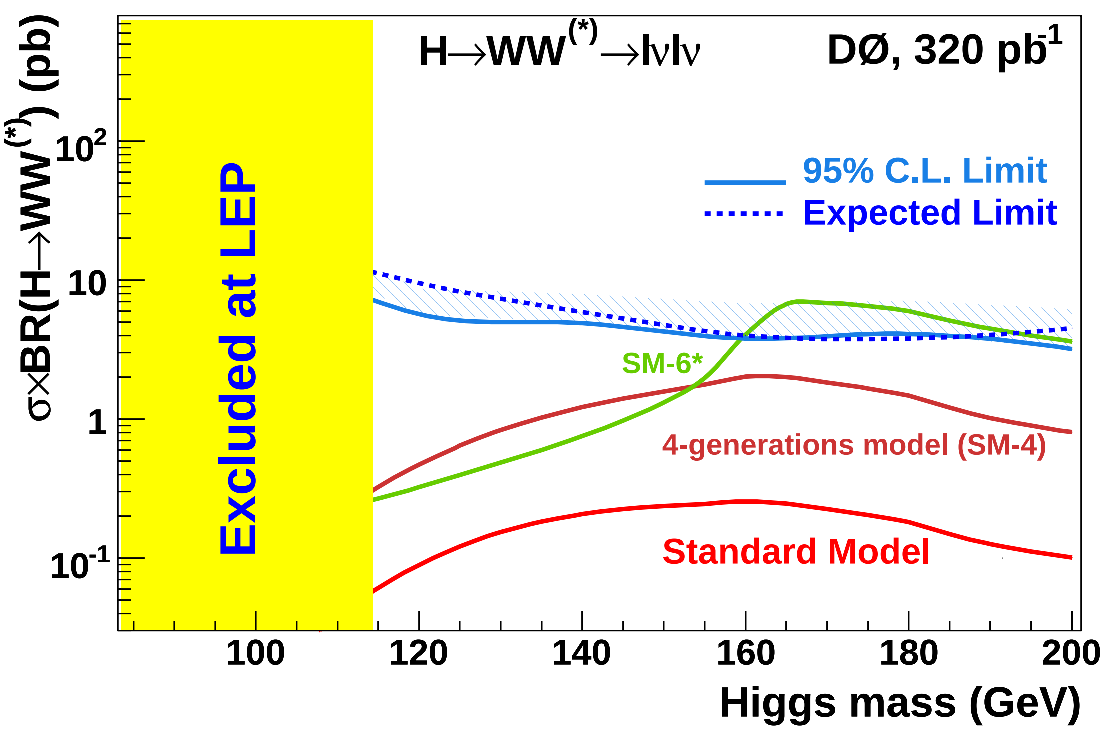

Figure 25: Excluded cross section times branching ratio $\sigma \times BR(H \to WW^{(*)})$ at 95% CL together with expectations from standard model Higgs boson production and alternative models derived using a Modified Frequentist approach. The LEP limit on the standard model Higgs boson production is taken from [39], the models with four (SM-4) and six generations (SM-6*) are presented in [40].

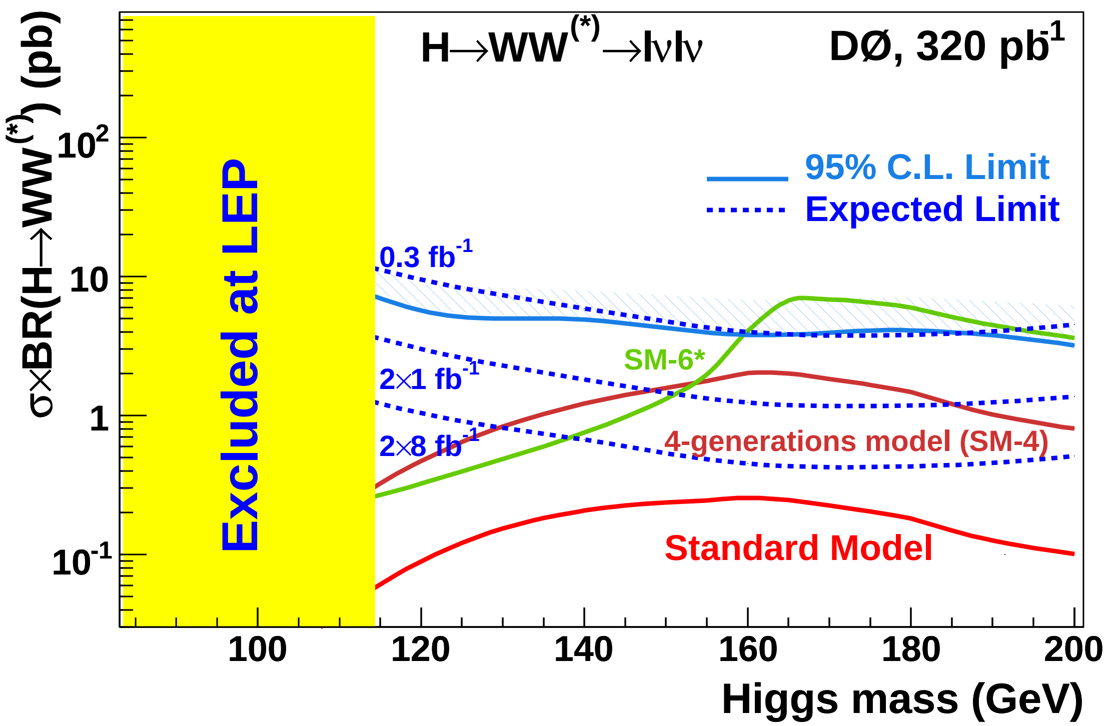

Figure 26: Excluded cross section times branching ratio $\sigma \times BR(H \to WW^{(*)})$ at 95% CL together with expectations from standard model Higgs boson production and alternative models derived using a Modified Fequentist approach and projected exclusion limits for 8 and 2×8 fb^{-1}. The LEP limit on the standard model Higgs boson production is taken from [39], the models with four (SM-4) and six generations (SM-6*) are presented in [40].

10 Conclusion

We have presented a search for the Higgs boson in $H \to WW^{(*)} \to \ell^+\nu\ell'^-\bar{\nu}$ $(\ell, \ell' = e, \mu)$ decays in $p\bar{p}$ collisions at a center-of-mass energy of $\sqrt{s} = 1.96$ TeV. The data, collected from April 2002 to June 2004 with the Run II DØ detector, correspond to an integrated luminosity of 325 pb^{-1} in the e^+e^-, 318 pb^{-1} in the $e^\pm\mu^\mp$ and 299 pb^{-1} in the $\mu^+\mu^-$ final state. The number of events observed is consistent with expectations from standard model backgrounds. Limits from the combination of all three channels on the production cross section times branching ratio $\sigma \times BR(H \to WW^{(*)})$ are presented. Alternative models with six generations of quarks can be ruled out for Higgs masses between 160 and 200 GeV.

References

[1] M. Carena *et al.* [Higgs Working Group Collaboration], "Report of the Tevatron Higgs working group", hep-ph/0010338.

[2] The DØ Collaboration, S.Abachi *et al.*, "The DØ Upgrade: The Detector and its Physics", Fermilab Pub-96/357-E (1996)

[3] J. Elmsheuser and M. Hohlfeld, DØ Note 4540 and 4542.

[4] V. M. Abazov *et al.* [D0 Collaboration], arXiv:hep-ex/0410066.

[5] The LEP working group for Higgs Boson searchers, LHWG Note/2002-01.

[6] E. Arik *et al*, SN–ATLAS–2001–006.

[7] M. Spira, hep–ph/9801289.

[8] S. Eidelman et al., Phys. Lett. **B 592**, 1 (2004).

[9] Common sample group,
`http://www-d0.fnal.gov/Run2Physics/cs/index.html`

[10] M. Hohlfeld, DØ Note 4392.

[11] J. Elmsheuser, DØ Note 4386.

[12] U. Blumenschein, DØ Note 4678.

[13] C. Noeding, DØ Note xxxx,
`http://www-clued0.fnal.gov/~noeding/ana05/trilepton_draft4.pdf`

[14] I. Torchiani, DØ Note xxx,
`http://www-d0.fnal.gov/Run2Physics/d0_private/eb/Run2EB_032/SusyFeb2005_Ingo_v03.pdf`

[15] DØ EM–ID group, EM–ID certification
`http://www-d0.fnal.gov/phys_id/emid/d0_private/certification/welcome.html`

[16] J. Kozminski *et al.*, DØ Note 4449.

[17] Jet algorithm group,
`http://www-d0.fnal.gov/computing/algorithms/calgo/jet/jetID_p14.html`

[18] Certified Jet Energy Scale
`http://www-d0.fnal.gov/phys_id/jes/d0_private/certified/certified.html`

[19] M. Agelou et al., DØ Note 4512.

[20] T. Sjöstrand, Comp. Phys. Comm. 82 74 (1994).

[21] M.L. Mangano, M. Moretti, F. Piccinini, R. Pittau, A. Polosa, JHEP 0307:001 (2003), hep-ph/0206293 (2002).

[22] CTEQ Collab., H. L. Lai et al., Phys. Rev. D55 1280 (1997).

[23] R. Hamberg, W. L. van Neerven and T. Matsuura, Nucl. Phys. B 359 343 (1991) [Erratum-ibid. B 644 403 (2002)].

[24] J. M. Campbell, R. K. Ellis, Phys. Rev. **D 60** 113006, `hep-ph/9905386` (1999).

[25] F. Abe *et. al*, The CDF Collaboration, Phys. Rev. Lett. 78, 4537 (1997).

[26] N. Kidonakis and R. Vogt, Phys. Rev. **D 68** 114014 (2003).

[27] A. Djouadi et al., Comp. Phys. Commun. 108 (1998) 56, hep-ph/9704448.

[28] M. Spira, Report DESY T-95-05 (October 1995), hep-ph/9510347.

[29] B. Tiller, T. Nunnemann, DØ Note 4660.

[30] S. Jain, DØ Note 4402.

[31] R. Stroehmer, `http://www-d0.hef.kun.nl///FullAgenda?phpida=a042017`

[32] DØ EvtGen Webpage
`http://www-d0.fnal.gov/computing/MonteCarlo/generator_tools/evtgen.html`

[33] DØ d0_mess Webpage
`http://www-d0.fnal.gov/computing/MonteCarlo/generator_tools/d0_mess.html`

[34] A. Pukhov et al.
CompHEP - a package for evaluation of Feynman diagrams and integration over multi-particle phase space, hep-ph/9908288.

[35] K. Hagiwara et al., Review of Particle Physics, Physical Review D 66, 010001 (2002).

[36] S. Anderson *et. al*, DØ Note 4116.

[37] T. Junk, Nucl. Instr. and Methods, **A 434** 435 (1999).

[38] I. Bertram *et al.*, "A recipe for the Construction of Confidence Limits", Fermilab-TM-2104.

[39] The LEP Working Group for Higgs Boson Searches, *Search for the Standard Model Higgs Boson at LEP*, CERN-EP/2003-011.

[40] E. Arik, O. Cakir, S.A. Cetin and S. Sultansoy, Phys. Rev. **D 66**, 033003 (2002). O. Cakir and S. Sultansoy, Phys. Rev. **D 65**, 013009 (2001).